CRUSTAL COMPOSITION BENEATH SOUTHERN IDAHO: INSIGHTS

FROM TELESEISMIC RECEIVER FUNCTIONS

by

Thomas Branson Harper

A thesis

submitted in partial fulfillment

of the requirements for the degree of

Master of Science in Geophysics

Boise State University

December 2018

Thomas Branson Harper

SOME RIGHTS RESERVED

BOISE STATE UNIVERSITY GRADUATE COLLEGE

DEFENSE COMMITTEE AND FINAL READING APPROVALS

of the thesis submitted by

Thomas Branson Harper

Thesis Title: Crustal Composition Beneath Southern Idaho: Insights from Teleseismic Receiver Functions

Date of Final Oral Examination: 29 August 2018

The following individuals read and discussed the thesis submitted by student Thomas Branson Harper, and they evaluated his presentation and response to questions during the final oral examination. They found that the student passed the final oral examination.

Lee M. Liberty, M.S.   Chair, Supervisory Committee

Dylan Mikesell, Ph.D.   Member, Supervisory Committee

Mark Schmitz, Ph.D.   Member, Supervisory Committee

The final reading approval of the thesis was granted by Lee M. Liberty, Chair of the Supervisory Committee. The thesis was approved by the Graduate College.

DEDICATION

I would like to dedicate this thesis to my family. Specifically, my parents and grandparents who taught me the values of education. Without their guidance, I would not be where I am today, doing what I love.

ACKNOWLEDGEMENTS

I would like to give special thanks to my thesis advisor, Lee Liberty, who taught me not only about Geophysics, but how to be a better scientist. His guidance and insights towards my research helped me learn how to tackle a scientific problem and how to best convey my methods. I learned a lot with my time at Boise State.

Secondly, I would like to acknowledge Dr. William Menke of Lamont-Doherty Earth Observatory. He gave me an opportunity to perform geophysical research as an undergraduate when I did not know much about the field. Without that chance, I doubt I would have learned how much I love this area of science. It also gave me the opportunity to pursue future endeavors in my life.

Lastly, I would like to thank my friends in Boise, Idaho. First and foremost, is my girlfriend, Tori Long, who made the sacrifice to move across the country so that I could pursue my education. There are also the friends of the ERB who were always there to offer their advice and jokes, making graduate school a lot less stressful than it could have been. Lastly, are the hooligans I met when I first moved to Boise. They are friends that I can count on for just about anything.

ABSTRACT

Receiver functions derived from teleseismic earthquakes contain seismic amplitude and velocity information that relate to compositional changes within the Earth's crust and upper mantle. The receiver function waveform is a combination of P-S converted waves that have reverberated within the lithosphere. Although the largest seismic velocity boundary is found at the base of the crust, I explore the use of lower amplitude receiver function arrivals that represent smaller velocity contrasts within the crust. In my thesis, I calculate and model receiver functions via a Metropolis algorithm approach to extract seismic velocity distributions in the lithosphere. I use the results to explore changing lithologies and heat signatures beneath the geologically complex southern Idaho region. In addition to a robust crustal thickness estimate for my study area, I show anomalously thick crust beneath the 14 Ma track of the Yellowstone hotspot compared to the surrounding regions, a thinner crust beneath the Oregon-Idaho graben and the Basin and Range province, and a distinct boundary between the Basin and Range and middle Rocky Mountains provinces. I highlight a high velocity zone between 6-14 km depth that is consistent with the presence of mid-crustal sills beneath the hot spot track, partial melt within the Yellowstone caldera, and relatively low velocities at seismogenic depths within the tectonic parabola of eastern Idaho. Anomalously slow velocities in the lower to mid-crust beneath the southern margin of the western Snake River Plain are coincident with high heat flow values and high total magnetic values, offering the possibility of mid-lower crustal partially melted dikes or sill complexes. I

utilize legacy active source refraction data to compare with receiver function results to further constrain seismic velocities. Overall, I find that receiver function analyses using a Metropolis algorithm inversion approach to estimate seismic velocity distributions show results below 6 km that are consistent with other studies. This approach offers the possibility of complimenting large-scale refraction experiments with low-cost receiver function analysis by utilizing earthquake waveforms from both permanent and temporary seismic deployments to constrain mid to lower-crustal properties. I discuss the use of this method as a tool for geothermal exploration by constraining crustal lithologies and identifying the presence of partial melt.

TABLE OF CONTENTS

LIST OF TABLES

LIST OF FIGURES

LIST OF ABBREVIATIONS

IRIS DMC   Incorporated Research Institutions for Seismology Data

Management Center

SRP   Snake River Plain

OIG   Oregon-Idaho Graben

WE   Weiser Embayment

BFZ   Brothers Fault Zone

IB   Idaho Batholith

WISZ   Western Idaho Shear Zone

HLP   High Lava Plains

CRB   Columbia River Basalts

UTEP PACES   University of Texas at El Paso Pan American Center for Earth and

Environmental Studies

R Reflection Coefficient

ρ Density

V Velocity

EARS   Earthscope Automated Receiver Survey

CHAPTER ONE: INTRODUCTION

Receiver function analysis is a seismic method to extract P-S converted seismic waves that have reverberated within the Earth's lithosphere. A standard receiver function objective is to extract crustal thickness by comparing travel time delays between the initial p-wave and converted s-waves produced from the high velocity contrast Moho, while ignoring other reflected or converted signals. By employing a Markov Chain Monte Carlo receiver function inversion technique known as the Metropolis algorithm, I extract seismic velocity distributions within the crust beneath southern Idaho using receiver functions. To date, physical property estimates for this region have been obtained by large scale, active source seismic surveys and by focused seismometer deployments. I show that a receiver function approach using past temporary and permanent deployment seismic data is a cost-effective way of characterizing large-scale earth structure within the crust.

The crust beneath southern Idaho and the surrounding regions contain a complex geology (Figure 1). Geologic provinces span Proterozoic North American lithosphere and the accreted terranes, and include granitic rocks of the Cretaceous Idaho Batholith, Neogene and younger sedimentary rocks of the Basin and Range, Neogene and younger volcanic rocks along the track of the Yellowstone hotspot, and Pliocene and younger lacustrine and fluvial deposits mostly beneath the western Snake River Plain (SRP). This complexity makes southern Idaho an ideal and challenging location to characterize crustal velocity distributions through receiver function analysis.

By utilizing the large seismic database available through the Incorporated Research Institutions for Seismology Data Management Center (IRIS DMC), I analyze receiver function waveforms to map seismic velocities in the crust. I use these results to highlight geologic province characteristics and specifically to 1) explore for partial melt materials to identify the source of high heat flow signatures, 2) compare the distribution of mapped mafic and felsic intrusive bodies beneath the SRP to measured seismic velocities, 3) characterize seismically active regions of southern Idaho at hypocentral depths of about 10-15 km, and 4) compare seismic velocity distributions to mapped geothermal resources that have a surface or near surface high heat flow expression.

My thesis begins by discussing the geology of southern Idaho and my motivation to investigate seismic velocity distributions within the crust. In Chapter 2, I review receiver function theory and discuss my approach to extracting receiver functions to estimate crustal structure. In Chapter 3, I explore the results from receiver function inversions where the output velocity tomograms are used for analysis. In Chapter 4, I utilize the velocity tomograms to constrain Moho depth or crustal thickness, explore mid-crustal seismic velocities in regions of high seismicity, explore for mafic intrusions and compare to other geophysical and geological studies, and compare seismic properties to regions where high heat flow has been previously identified. Lastly, I compare my results, in cross section, to active source legacy seismic refraction results. I show comparable results for velocity distributions within the crust and conclude that by utilizing earthquake data, rock and fluid properties can be assessed beneath southern Idaho and surrounding areas without the expense of active source approaches.
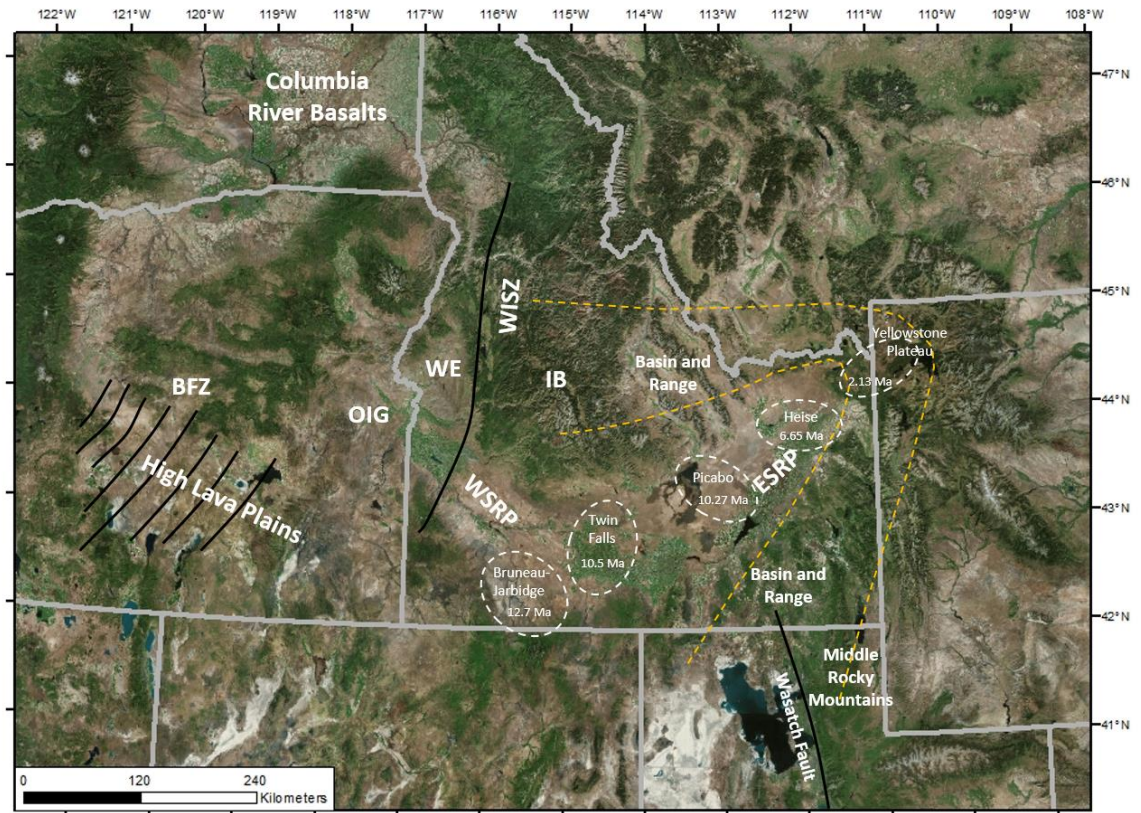
Figure 1.   **Map of northwest United States showing the general location of select geological features. Shown in the map are the Columbia River Basalts, High Lava Plains, Western SRP (WSRP), Eastern SRP (ESRP), caldera centers of the Yellowstone hotspot (white dashed ovals) and their corresponding ages derived from Anders et al. (2014), Tectonic Parabola (orange parabolic dashed lines with the head at Yellowstone), Oregon-Idaho Graben (OIG), Weiser Embayment (WE), Brothers Fault Zone (BFZ) (black lines near High Lava Plains),Western Idaho Shear Zone (WISZ) (black line), Idaho Batholith (IB), Yellowstone, the Basin and Range province, Wasatch Fault (black line), and Middle Rocky Mountains province.**

Geologic and Geophysical Setting: Pre-Snake River Plain

Prior to Miocene basin formation related to the formation of the SRP, many geologic events shaped the surrounding region. The Idaho Batholith formed during the Cretaceous period, in response to the subduction and accretion of the oceanic Farallon plate under the continental North American plate, causing the oceanic plate to melt and mix with underlying mantle rocks. This melt generated the felsic plutons that slowly rose

and crystallized in the crust, causing uplift and producing the granitic composition of the batholith (Hyndman, 1983). The 20-25 km thick Idaho Batholith is the cratonic core of the region, located in central Idaho, north of the western/central SRP (Figure 1; e.g., Davenport et al., 2017).

The boundary between the North American craton and the accreted Blue Mountains province is located near the western border of Idaho and is termed the western Idaho Shear Zone (WISZ) (Figure 1). This 5 km wide, right-lateral transpressional lithospheric boundary strikes N-S (Giorgis et al., 2008), and separates the accreted oceanic terranes with $^{87}Sr/^{86}Sr$ values less than 0.704 from the plutons of the North American craton with $^{87}Sr/^{86}Sr$ values greater than 0.707 (Manduca et al., 1992). The initiation of the WISZ began about 105 Ma and ended around 90 Ma (Manduca et al., 1993; Giorgis et al., 2005; Giorgis et al., 2008).

Using receiver function methods, Stanciu et al. (2016) examined crustal thickness across the WISZ, utilizing the 85 seismometers from the EarthScope Idaho-Oregon experiment that spanned from the Blue Mountains province to the North American craton in Idaho. Using the H-k grid search method and common conversion point stacking (described in Chapter 2), they imaged a decrease in crustal thickness from 28 km west of the WISZ to 36 km to the east. Davenport et al. (2017) studied the crustal structure along the same line using active source refraction and wide-angle reflection methods. The results showed similar findings when compared to the receiver function analyses where the WISZ was near vertical, with a 7 km increase in crustal thickness to the east of the WISZ. Davenport et al. (2017) also imaged a high velocity crustal layer west of the

WISZ, interpreted as mafic underplating associated with the feeder system of the Columbia River basalts (CRB).

The Basin and Range province is the next oldest geologic landform in the region and is bisected by the eastern SRP (Figure 1). This province results from extension and thinning of the lithosphere, producing a high mountain horst and basin-forming graben setting. The beginning of extension within the Basin and Range province varies over the different regions. It is believed that extension began north of the eastern SRP at about 55-49 Ma across the Idaho Batholith and south of the eastern SRP between 38-20 Ma (Wernicke et al. 1987). Extension continues to present day, as evidenced by high seismicity rates and a unique geodetic signature.

West of the SRP lies the High Lava Plains (HLP) province, which is an age-progressive, bimodal volcanic terrane (Jordan et al., 2004; Streck and Grunder, 2008), estimated to contain 220,000 km^3 of basalt (Camp and Ross, 2004) (Figure 1). The history of the HLP includes back arc volcanism at 30 Ma, ignimbrite flare-up of silicic magmas from 20-25 Ma, flood basalt volcanism at 16-17 Ma, and volcanism from the Newberry volcano and Yellowstone hotspot around the same time (Carlson and Hart, 1987; Hart and Carlson, 1987; Jordan et al., 2004; Brueseke et al., 2007; Streck and Grunder, 2012).

Cox et al. (2013) produced crustal models of the HLP region using an integrated approach of controlled source seismic, gravity, and geologic constraints. They showed that the HLP crust is very similar to that of the Basin and Range province to the south, comprised of a thinner crust than the surrounding continental crust. A layer of sedimentary and volcanic rocks that reaches a thickness of 5-7 km overlies most of the

HLP crust. Evidence of mafic intraplating and underplating were also observed within the HLP region.

Eager et al. (2011) performed receiver function analyses to image the crustal structure of the HLP region using 206 seismic stations to perform both H-k stacking and Gaussian-weighted common conversion point stacking. They noticed a change in Moho from 40 km depth beneath the Cascades, Idaho Batholith, and Owyhee Plateau, to 31 km depth beneath the HLP and northern Great Basin (Figure 1). They observed abnormally high Poisson's ratios (~0.320) and low crustal velocities beneath north-central and southern Oregon, consistent with the presence of mafic partial melt at the mid to lower crust. Eager et al. (2011) suggested that there was a central zone where melts had drained to the surface, possibly assisted by the Brothers Fault Zone (Figure 1).

Volcanism initiated in southeast Oregon around 17.5 Ma to 15.5 Ma with the massive CRB eruption and scattered rhyolitic volcanism (Hooper and Swanson, 1990; Clemens and Wood, 1991) (Figure 1). These volcanic rocks extended south into the northern part of the western SRP and as far as northern Nevada. The CRB initiation has also been connected to the Yellowstone mantle plume initiation (Geist and Richards, 1993).

North of the western SRP lies the Weiser embayment. This basin contains an accumulated 2.1 km of basalt dated to be older than 15 Ma (Hooper and Swanson, 1990; Fitzgerald, 1982; Hooper and Hawkesworth, 1993). Slightly west of the western SRP lies the 15.5 – 10.5 Ma Oregon-Idaho graben (Cummings et al., 2000). Both of these basins contain north-south trending faults, and are postulated to have been one basin prior to the initiation of western SRP extension (Wood and Clemens, 2002).

Geologic and Geophysical Setting: Snake River Plain

Around 11-8.5 Ma, volcanism related to the passage of the Yellowstone hotspot began to localize around the Bruneau-Jarbidge eruptive center (Figure 1) (Bonnichsen et al., 1989). This eruptive center presumably marks the beginning of focused volcanism along the track of the Yellowstone hotspot produced by both thermal expansion and subsequent contraction that manifest today as a topographic depression when compared to the surrounding regions. Continued volcanism along the hot spot track has produced the low topography expression of the eastern SRP that follows North America plate motions (Figure 1).

The western SRP is interpreted as a structural graben that trends about N42W. The heating of the lithosphere from the injection of large amounts of basaltic magma into the mid-crust, presumably from hotspot interaction, initiated western SRP extension around 11-8.5 Ma. This basalt also added a considerable amount of weight and in turn, caused upper crustal subsidence (Baldridge et al., 1995; Wood and Clemens, 2002).

Based on deep drill holes in the western SRP, there is a lack of hot spot derived rhyolite in the center of the western SRP (Lewis and Stone, 1988; Clemens, 1993), whereas 2-km layers of rhyolite have been mapped along the margins of the plain (McIntyre, 1979; Ekren et al., 1981; Wood, 1989; Clemens and Wood, 1993). This suggests that the plain was an upland during the rhyolitic Bruneau-Jarbidge eruptions. Normal faulting that is associated with western SRP extension had slip rates of 0.5 mm/year from 11-9 Ma, producing roughly 2 km of structural downwarping. Since 9 Ma, the average slip rate has lowered to 0.01 mm/year, dropping the basin a total of 0.3 km

with respect to the margins (Wood and Clemens, 2002). Thus, low seismicity rates are observed along the western SRP margins.

Upon formation, the western SRP was a closed depocenter that filled with lake sediments as early as 10 Ma (Wood and Clemens, 2002). Between 6–4 Ma, lake levels rose upwards of 1000 meters (Squires et al., 1992), producing Paleozoic Lake Idaho. Then, around 4 Ma the lake rose to the level of the surrounding hills, and downcut the present-day Hells Canyon to drain the lake. These lake events left roughly 2 km of lacustrine sediments in the western SRP superimposed on, and interbedded with, the Miocene and younger basalts.

Basaltic volcanism in the western SRP resumed approximately 2.2 Ma in the form of shield volcanoes, to as recently as 100,000 years ago (Bonnichsen et al. 1997), emplacing roughly 300 cubic km of material (Whitehead, 1992). These shield volcanoes occurred along the west-trending 100 km long Kuna-Mountain Home volcanic-rift zone. This rift has an oblique orientation with respect to the western SRP and may be responsible for high heat flow identified in the region (Shervais et al. 2015).

To image the crust of the western SRP and surrounding region, Hill and Pakiser (1967) performed a seismic refraction survey using underground explosions over a 454 km line extending from Eureka, Nevada to Boise, Idaho (Figure 2). Their interpretations involved a rather thin crust beneath the northern Basin and Range province of northern Nevada, having a Moho at ~30-35 km depth. Beneath the western SRP, a 5.2 km/s layer was interpreted from the surface to ~9 km depth and then a 6.7 km/s layer extending to the Moho around 44 km depth. This dataset was reinterpreted by Prodehl (1979) through

forward modeling, showing similar results as Hill and Pakiser (1967) except average

crustal velocities beneath the SRP were found to be higher.
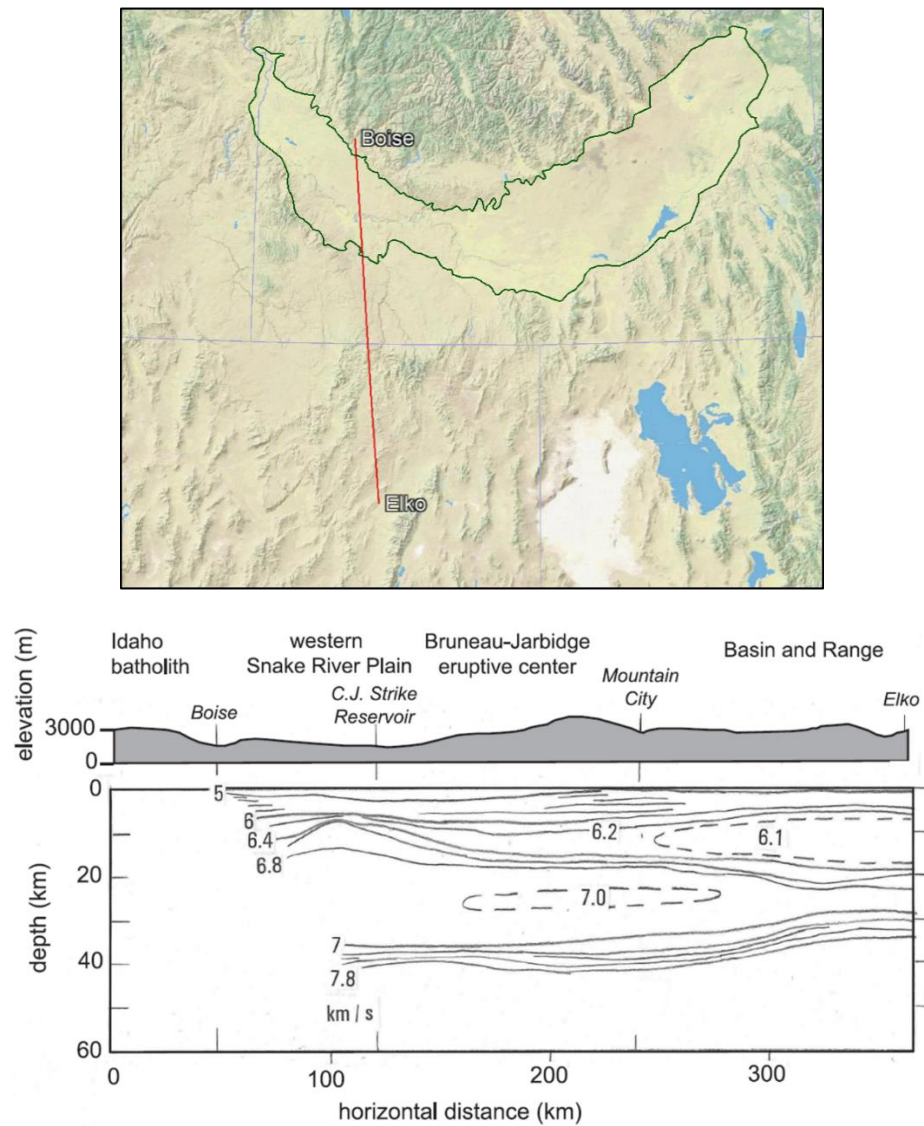
Figure 2.   Top: Location of Hill and Pakiser's 1962 refraction survey extending from Boise, ID to Elko, Nevada. The outline of the topographic expression of the SRP is in green. Bottom: The Prodehl (1979) reinterpretation of Hill and Pakiser (1967) refraction data and crustal structure from Boise to Elko.

Unlike most continental extensional basins that are in-filled with low density

sediments, the western SRP displays a positive gravity anomaly of +25 to +60 milligals

and high magnetic anomalies and lineation's (Figure 3). These signatures represent

intrusive volcanic rocks emplaced within the crustal rocks of the Idaho Batholith (Hill, 1963; Khatiwada and Keller, 2017). Khatiwada and Keller (2017) performed an integrated analysis of this gravity and magnetic data to study the western and central SRP. Their final models show mid-crustal intrusions at depths of ~10-20 km in both the western and central SRP.
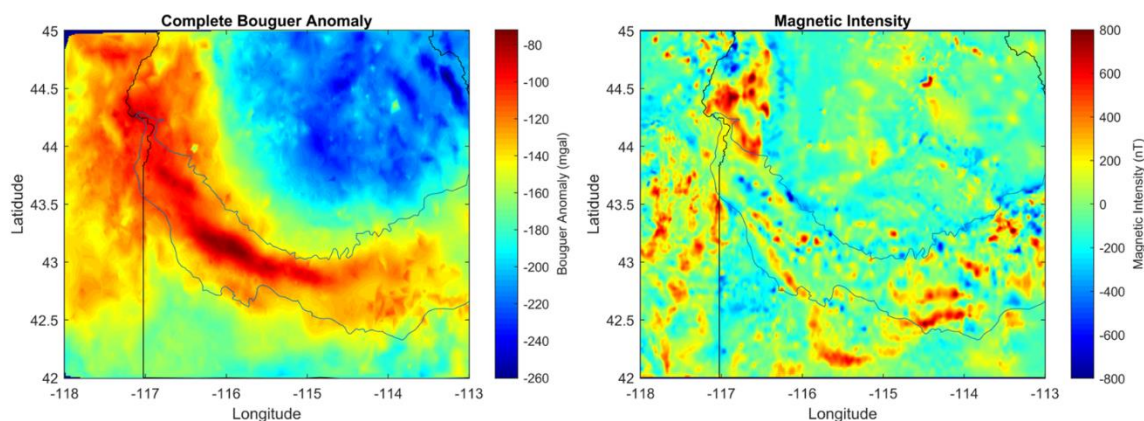
Figure 3. **Gravity and magnetic maps of the SRP and surrounding area derived from the University of Texas El Paso PACES database (http://gis.utep.edu/subpages/GMData.html last accessed February, 2017). Left: A map of complete Bouguer gravity. Right: A map of magnetic intensity.**

The eastern SRP is a structural downwarp connected to the passage of the mantle-derived Yellowstone hotspot, with the hotpot track migrating about N57E at roughly 2.34 cm/year with respect to the North American plate (Gripp and Gordon, 2002, Anders et al., 2014). Many studies have linked the age of past eruptive centers to hot spot interactions, consistent with the known plate velocity (Armstrong et al. 1975; Morgan et al. 1984; Bonnichsen et al. 2008; Anders et al., 2014).

A seismic refraction survey was performed in 1978 that showed a 10 km thick high velocity layer within the eastern SRP crust from 10-20 km depth (Priestley and Orcutt, 1982; Sparlin et al., 1982). This high velocity zone has been interpreted to be a mid-crustal sill complex. Peng and Humphreys (1998) made similar observations by

utilizing receiver functions. Stachnik et al. (2008) produced shear wave velocity models of the eastern SRP using Rayleigh wave dispersion and receiver functions. This study also located a mid-crustal sill complex, but found it to be deeper than previously thought, with the top at 15-20 km depth.

DeNosaquo et al. (2009) studied the eastern SRP by analyzing gravity data with additional constraints from geophysical and geological data. They offered evidence that the lower crust of the eastern SRP has been thickened by the addition of an underplated layer of high density/high velocity clinopyroxene. They also suggest that a thin layer of partial melt lies at the base of the lower crust and that dioritic mid-crustal sills are present that varies in thickness from 4-11 km, at a 10-20 km depth.

Yuan et al. (2010) performed receiver function analyses on the eastern SRP to determine Moho topography. This study provided two interesting results: (1) the crust beneath the eastern SRP is thickest beneath the young calderas (47 km) and thinnest beneath the older Twin Falls caldera (40 km); (2) the crust beneath the plain was typically 4 km thicker than the crust along the margins of the plain. Apart from examining Moho structure, they found evidence of lower crustal outflow beneath the eastern SRP, caused by the injection of dense magmatic materials.

Geologic and Geophysical Setting: Lithospheric Signature of the Snake River Plain

The Yellowstone mantle plume geometry has been imaged in many studies using passive-source seismic methods. Yuan and Dueker (2005) performed P-wave traveltime tomography to image a 100 km diameter mantle plume that extends 500 km deep, dipping at 20 degrees from vertical to the northwest. The velocity perturbations of this plume were measured to be -3.2% at 100 km depth to -0.9% at 450 km depth, suggesting

a uniform 180°C increase in thermal temperatures. This velocity to temperature

relationship is based on the idea that as a rock is heated to its melting point, the seismic

velocity will rapidly decrease (Schmitz et al., 1997).

Smith et al. (2009) studied the Yellowstone hotspot by integrating geophysical

and geological data. They also found that the hotspot dips, but to the WNW at 30 degrees

from vertical to 660 km depth. Slow seismic velocities revealed that a magma reservoir

of 8% - 15% partial melt lies in the mid-crust beneath the Yellowstone caldera. Based on

their findings of the current hotspot geometry, they extrapolated the plume to its original

location at 17 Ma and found a connection to the High Lava Plains basalt field, suggesting

a common mantle plume source.

Nelson and Grand (2018) used shear wave travel time tomography to image the

deeper roots of the Yellowstone mantle plume. They found that the plume initially tilts to

the North, and then dips to South starting at about 500 km depth towards the core mantle

boundary. Assuming this is a thermal anomaly, the excess temperature in the deepest part

of mantle is calculated to be 650-850°C.

Many published tomograms are available at the IRIS DMC (2011) that utilize the

USArray seismic data. Similar to how previous studies have looked for low velocity

zones to characterize the melt geometry of the Yellowstone hotspot plume, I use these

data to examine velocity distributions along the relic hotspot track to characterize the

crustal structure and presence of partial melt along the passage of the hotspot. For this

study, I utilize the IRIS DMC (2014), DNA13 Earth model

(https://ds.iris.edu/ds/products/emc-dna13/ last accessed January, 2017), which is a

velocity perturbation dataset. This dataset is most useful because of the dense regional station coverage and the velocity perturbations are valuable for the goals of this project.

The DNA13 Earth model is utilized here to define crustal and mantle velocity anomaly distributions along the relic Yellowstone hotspot track. This Earth model is a joint inversion of teleseismic body-wave traveltime and surface-wave phase velocity measurements to constrain body wave (P, SV), and surface wave (SH) wave velocities (Porritt et al., 2014). The station coverage includes the USArray transportable array, regional seismic networks, and temporary seismic deployments. The recorded data includes 400 events for teleseismic body waves, 167 events for phase velocity measurements, and 5 years of ambient noise, recorded from January 2007 to December 2012.

Figure 4 shows P-wave perturbation cross section slices from the DNA13 dataset to a depth of 150 km. The Yellowstone mantle plume is clearly observed in slice C-C', D-D', E-E', and F-F' by its distinct low velocity mantle signature (below 40 km depth) that reaches a maximum perturbation of roughly -1 %. Assuming the lower velocity zone represents a region of melt produced by the hotspot plume, I use this as a proxy for finding other regions of partial melt that have been emplaced throughout time. One interesting shallow feature is located along line B-B', where we see a slow velocity anomaly at 10-25 km depth (red box). This anomaly has a high amplitude of negative velocity perturbation with a value of -0.47 %.
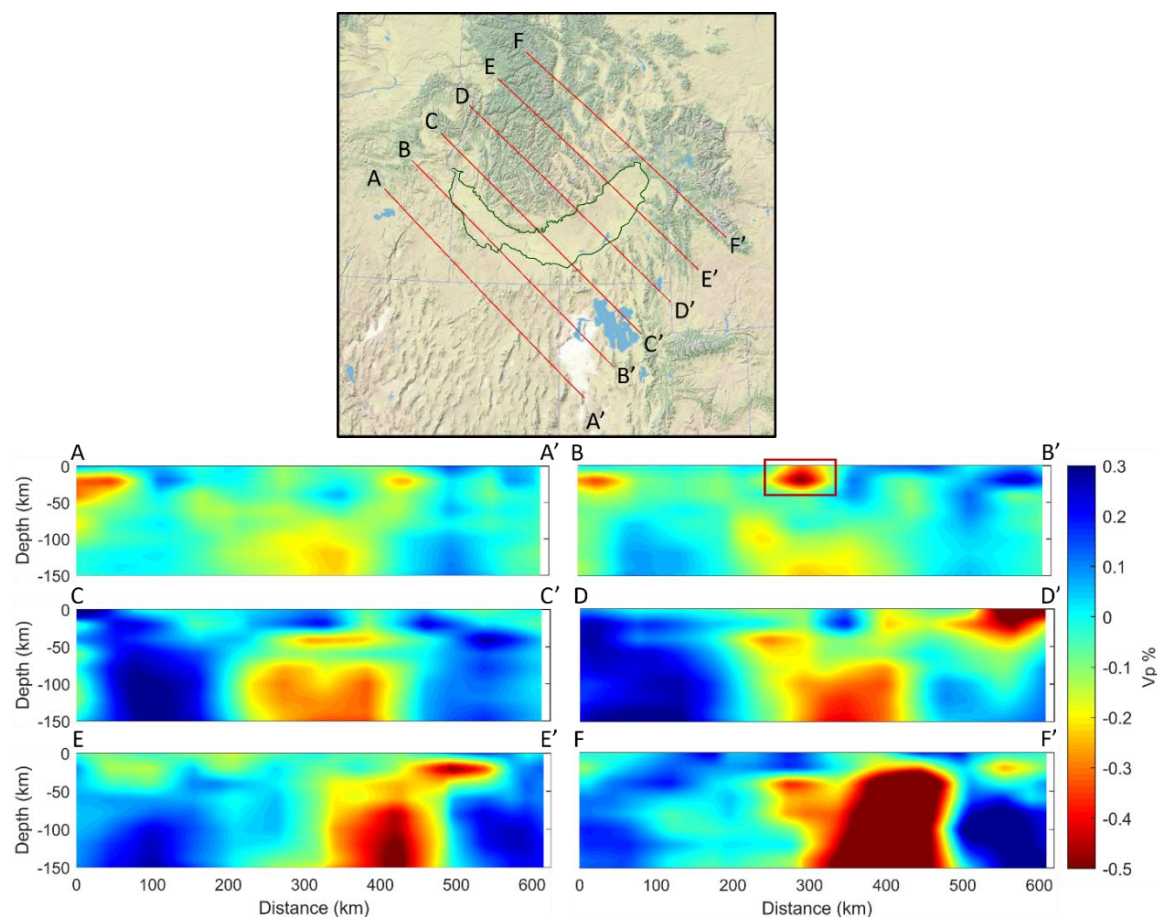
Figure 4. Top: Map of the study area with red lines denoting the locations of the cross section slices. The green outline represents the boundary of the SRP. Bottom: Cross section slices of the cross sections. The geometry of the relic Yellowstone hotspot is represented by the slow velocity zone cutting through the lithosphere. The red box in slice B-B' represents the slow velocity anomaly observed at shallow depths. Note the decrease in Vp% beneath the topographic expression of the eastern SRP across the northern cross sections.

Geothermal energy

Largely in part to abundant Neogene and younger volcanism, southern Idaho is a region of high heat flow where geothermal resource extraction is feasible (Blackwell, 1989). Similar to how a coal power plant is operated to create energy, geothermal power plants use hot fluids extracted from the ground to create high-pressure steam, that spins a turbine to produce electricity. Because heat sources are typically located at great depths, two variables are needed to efficiently tap geothermal energy: (1) a sustainable heat

source to produce 150–400 °C temperatures and (2) permeability to deliver deep heated water to marketable production depths. There are currently two operating geothermal power plants near the SRP region; (1) Neal Hot Springs with reservoir temperatures of 141 °C (Warren, 2017) and (2) Raft River with reservoir temperatures of 149 °C (Bradford et al., 2013). By relating high heat flow areas beneath southern Idaho to seismic velocity distributions, additional geothermal resources could be recognized and exploited.

Heat flow and geothermal resources of southern Idaho

Many studies have suggested the emplacement of sill complexes within the crust of the SRP (e.g., Hill and Pakiser, 1967; Prodehl, 1979; Braile et al., 1982; Priestley and Orcutt, 1982; Smith et al., 1982; Sparlin et al., 1982; McQuarrie and Rodgers, 1998; Peng and Humphreys, 1998; Christiansen, 2001; Shervais et al., 2006; Stachnik et al., 2008). Most of these sill complexes have likely been emplaced either through direct passage of the Yellowstone hotspot or through residual heat processes. It is plausible that these old sill complexes could still contain residual heat that could account for the SRP being one of the highest heat flow provinces in North America (Blackwell, 1989). Fleischmann (2006) estimated that the SRP volcanic province could contain up to 855 MW of geothermal power production.

To identify high heat sources, Shervais et al. (2016) compiled heat distributions based on measured thermal gradients, interpolated heat flow values, groundwater temperatures, the distribution of volcanic vents (weighted by age, size, and composition), measured temperatures of thermal waters from springs and wells, calculated ionic and multicomponent temperatures of thermal waters from springs and wells, and the

distribution of high ^{3}He/^{4}He in thermal waters (Figure 5). The sources of these heat

anomalies are interpreted to be from partial melt, mafic sills, or from radiogenic

processes related to the Idaho Batholith. In some cases, these heat sources may be mixed

or undetermined. Because seismic velocities are heat and pressure dependent (i.e.,

sensitive to rock and fluid phases at a range of depths), I use seismic velocity analyses to

identify and characterize heat sources for southern Idaho. The challenge is to separate

changing rock chemistry from temperature effects (e.g., Christensen and Mooney, 1995).

To identify the exact partial melt percentage of these low velocity anomalies is a

difficult task. Many variables must be considered to estimate partial melt percentage such

as lithology, grain boundary size, water content, depth, density, etc., and therefore was

outside of the scope of my thesis. DeNosaquo et al. (2009) provided a velocity-density

plot for rocks in the SRP volcanic field (Figure 6), which I will use to constrain rock

properties from seismic velocities.
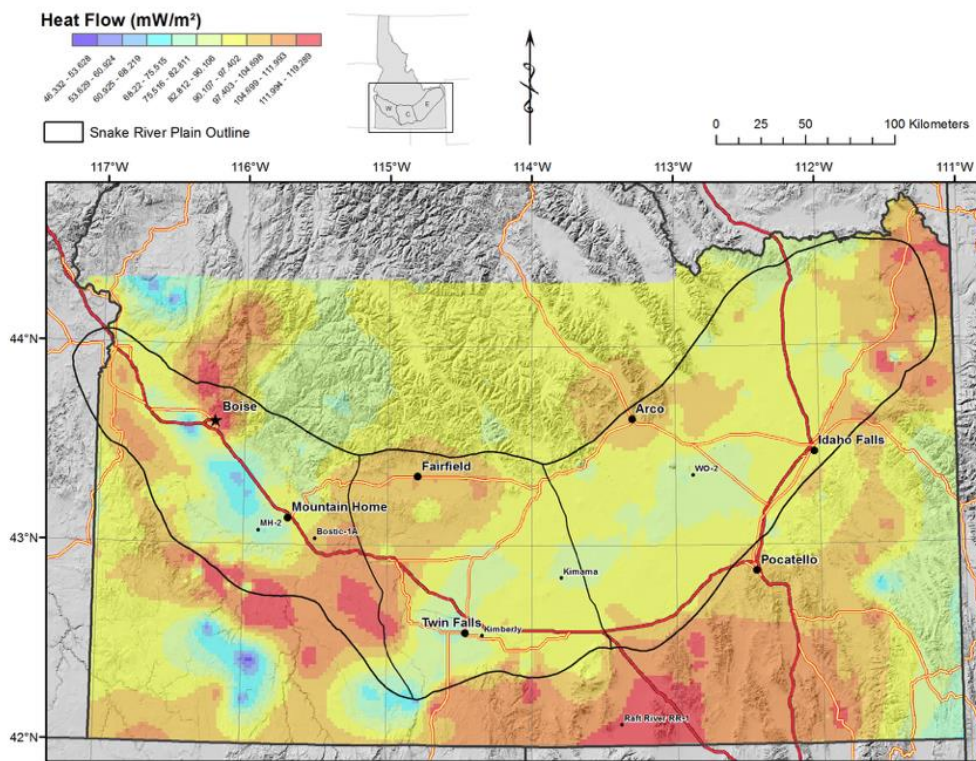
Figure 5. **Heat flow estimates of southern Idaho through the Empirical Bayesian Krige function approach from Shervais et al. (2015). The map is based on measured thermal gradients, interpolated heat flow values, groundwater temperatures, the distribution of volcanic vents (weighted by age, size, and composition), measured temperatures of thermal waters from springs and wells, calculated ionic and multicomponent temperatures of thermal waters from springs and wells, and the distribution of high ^{3}He/^{4}He in thermal waters. The sources of these heat anomalies are interpreted to be partial melt, mafic sills, and radioactive decay of the Idaho Batholith.**
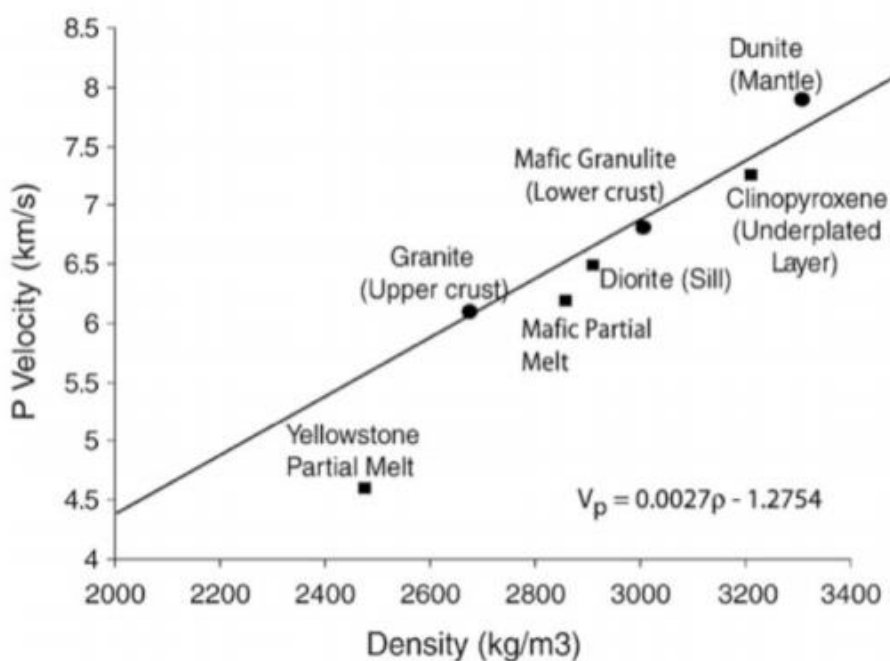
Figure 6. **Velocity–density plot for select rocks in the SRP volcanic field. Figure is from DeNosaquo et al. (2009).**

Mabey (1983) compiled reservoir temperature data and defined different geothermal areas and systems in Idaho (Figure 7). These geothermal systems (excluding Neal Hot Springs) and their estimated mean reservoir temperatures (Table 1.1) are from Young and Mitchell (1973), Brook et al. (1979), and Muffler and Guffanti (1979). The Neal Hot Springs data is from Warren (2017). Below, I summarize a few of these systems that I will compare to my seismic results.

In the Weiser area, there are a high number of high temperature geothermal systems. Miocene sedimentary rocks and basalt underlie this area, with hot springs along northwest trending fault zones (Mabey, 1983). The Neal Hot Springs geothermal system is already a power plant producing 30 MW annually (Warren, 2017; Figure 7, number 6). The Crane Creek-Cove Creek system was explored in 1981, drilling to 7,998 feet and finding a temperature of 162.8°C (Figure 7, number 2). Although this was an attractive

temperature for a power plant, insufficient amounts of water prohibited the development of a facility (Neely and Galinato, 2007).

In southeastern Idaho, there is another dense population of geothermal systems likely created by Basin and Range extension that thins the crust. The Raft River Area geothermal plant is located here and produces 11 MW annually (Bradford et al. 2013; Figure 7, number 18).

In the western SRP, the Bruneau-Grand View geothermal system holds the largest mean reservoir volume in Idaho of 1830 km^3 (Brook et al. 1979; Figure 7, number 12). This area contains complex geologic structure due to the history of region. Most of the surface comprises of lacustrine sediments with regions of basalt flows. The 3.4 km deep Anshutz Corporation well drilled in 1974 reached a temperature high of 147.8°C and the 2.67 km deep Phillips Petroleum Company well drilled in 1978 measured a temperature high of 107.8°C. The sources of this high heat flow region are unknown but is most likely connected to the mafic intrusions that lie beneath the western SRP. It is possible that the shallow low velocity zone observed in line B-B' of Figure 4 is mid-crustal partial melt that is the source of this high heat flow region.

Overall, southern Idaho is a region of high heat flow, largely in part to the passage of the Yellowstone hotspot. The sources of these high heat flow values are not fully understood and can be better constrained by measuring seismic velocities within the region. By doing this, I may be able to better quantifying geothermal resources in the area.
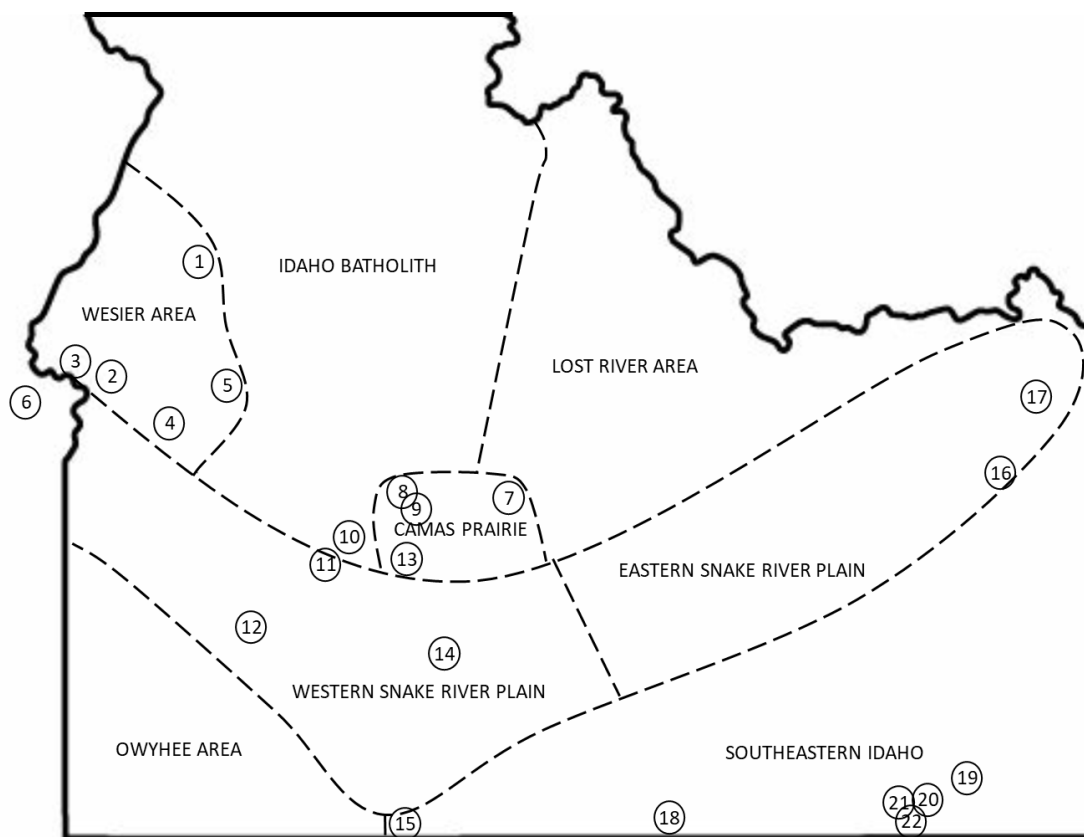
Figure 7. Map of southern Idaho showing geothermal areas defined by Mabey (1983). The numbers correspond to the geothermal systems in Table 1.

Table 1.1 **Names of the geothermal systems in southern Idaho and their estimated mean reservoir temperature.**

No.	System	Estimated Mean Reservoir Temperature °C
1	White Licks Hot Springs	139
2	Crane Creek-Cove Creek	171
3	Weiser area	130
4	Roystone Hot Springs	135
5	Payette River area	131
6	Neal Hot Springs	141
7	Magic Reservoir area	149
8	Wardrop Hot Springs	97
9	Barron's Hot Springs	103
10	Latty Hot Springs	124
11	Radio Towers area	125
12	Bruneau-Grand View area	107
13	White Arrow Hot Springs	103
14	Banbury area	117
15	Murphy Hot Springs	103
16	Newdale area	100
17	Ashton Warm Springs	92
18	Raft River Area	149
19	Maple Grove Hot Springs	93
20	Riverdale area	99
21	Wayland Hot Springs	113
22	Squaw Hot Springs	119

CHAPTER TWO: DATA AND METHODOLOGY

Receiver Functions

Three-component seismic stations record teleseismic earthquake waves that propagate through the Earth. Teleseismic earthquakes are defined as earthquakes that occur more than 1000 km from the station location, and typically contain usable signals at magnitude 5.5 or higher. The waveforms and associated travel times contain information about the earthquake source, the ray propagation path, the P-wave and S-wave seismic velocities along the propagation path, and the instrument response. The receiver function is the time window that contains signals from within the crust and upper mantle with instrument response and source characteristics removed through signal processing. This waveform is obtained by deconvolving the radial component with the vertical component of motion:

$$H(\omega) = \frac{R(\omega)}{Z(\omega)}$$

where R(ω) is the Fourier transform of the radial component (horizontal shear motion with a small p-wave contribution), Z(ω) is the Fourier transform of the vertical component (P-wave motion with a small contribution from vertically polarized shear waves), and H(ω) is the Fourier transform of the receiver function. The deconvolution removes all P-wave phases (except the initial arrival) and leaves behind the S-waves that have reverberated within the crust and upper mantle (Figure 8). For more information of

the receiver function process, see Langston (1979); Owens et al. (1984); and Ammon (1991).
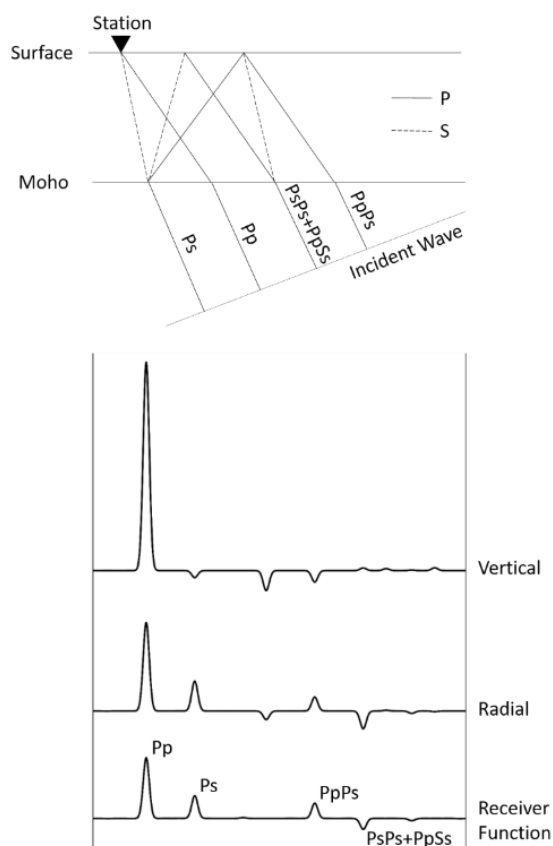
Figure 8.   Top: Simplified receiver function ray path diagram for a single layer crust. Bottom: Vertical and radial time series waveform response of the seismometer and the calculated receiver function for a single layer crust by deconvolving the radial signal from the vertical signal.

The receiver function waveform contains P-S converted waves that have reflected from high contrast velocity boundaries along the ray's travel path. For a simple two layer (crust/mantle) model, the receiver function would look like the bottom waveform in Figure 8. When analyzing this waveform, it is important to look at the arrival travel time and amplitude. The arrival times depend on boundary depths and emergence angles of the P and S signals. The amplitudes largely depend on reflection coefficients across velocity

and/or density boundaries, while also depending on the incidence angles. The reflection

coefficient is the amplitude of the reflected wave to the incident wave, and in the case of

normal (vertical) incidence, can be expressed as,

$$R = \frac{\rho_2 V_2 - \rho_1 V_1}{\rho_2 V_2 + \rho_1 V_1}$$

where,

$R =$ The reflection coefficient

$\rho_1 =$ Density of upper layer

$\rho_2 =$ Density of lower layer

$V_1 =$ Velocity of upper layer

$V_2 =$ Velocity of lower layer

Assuming constant density (or density ratio) across boundaries, this means that a

large velocity contrast will produce a large amplitude response with a positive amplitude

resulting from $V_2 > V_1$, and a negative amplitude resulting from $V_1 > V_2$. Although

receiver functions are very useful for determining large velocity boundaries that include

the crust/mantle interface or Moho (often greater than 15% increase), these same

waveforms can also be used for finding smaller velocity contrasts in the crust (less than

5% contrast).

Traditionally, crustal velocity distributions are obtained by active source

refraction surveys that require large explosions that can be difficult to permit. These

refraction surveys typically record signals with a seismic frequency between 10-20 Hz

with a dense array of geophones or seismometers. In contrast, earthquakes in my study

are filtered to a maximum seismic frequency of 5 Hz and typically recorded with fewer

seismometers. This results in my receiver function analysis having less than half the

vertical resolution as a typical refraction survey with lower spatial resolution. Here, I explore the limits of receiver function analysis to obtain detailed crustal velocity distributions.

Typical methods of analyzing receiver functions involve H-k stacking and common conversion point stacking. H-k stacking is a method to determine crustal thickness (H) and average Vp/Vs ratio (k) within the crust (Zhu and Kanamori, 2000). Common conversion point stacking back projects receiver function amplitudes using ray tracing to locate significant velocity discontinuities at depth (Dueker and Sheehan, 1997). In this study, I take a different approach by using receiver function waveforms to estimate the seismic velocity of the crust through an inversion approach.

Data

Through the USArray program, mapping the velocity structure of the Earth has been dramatically enhanced. This project began deploying seismometers throughout the United States in 2007 to better understand the crustal and mantle structures beneath the United States. With ~70 km station spacing across the country, infilled with local permanent seismic stations, high velocity anomalies such as subducting slabs (Obrebski et al., 2010), and low velocity anomalies like the Yellowstone plume (Obrebski et al., 2010; Yuan et al., 2010) or the Northern Appalachian Anomaly (Menke et al., 2016; Levin et al., 2018) have been imaged.

The majority of three-component, broadband seismometers used in this study are from the USArray (Red bullseyes in Figure 9). Other networks used include the USGS networks (Albuquerque, 1980), International Miscellaneous Stations, Intermountain West seismic network (Albuquerque, 2003), United States national seismic network

(Albuquerque, 1990), University of Utah Regional seismic network (University of Utah, 1962), Pacific Northwest seismic network (University of Washington, 1963). Focused deployment datasets include data from the Yellowstone Wyoming seismic network (University of Utah, 1984), HLP network (James and Fouch, 2006), Yellowstone Hotspot network (Dueker et al. 2000), Shear-wave Splitting in the Snake River Plain (Walker and Klemperer, 2000), DeepProbe (Dueker and Humphreys, 1997), Montana broadband array, Ruby Range core-complex (Klemperer and Miller, 2010), and the Boise Fort Noise observation (Xu, personal comm.) (White bullseyes in Figure 9).
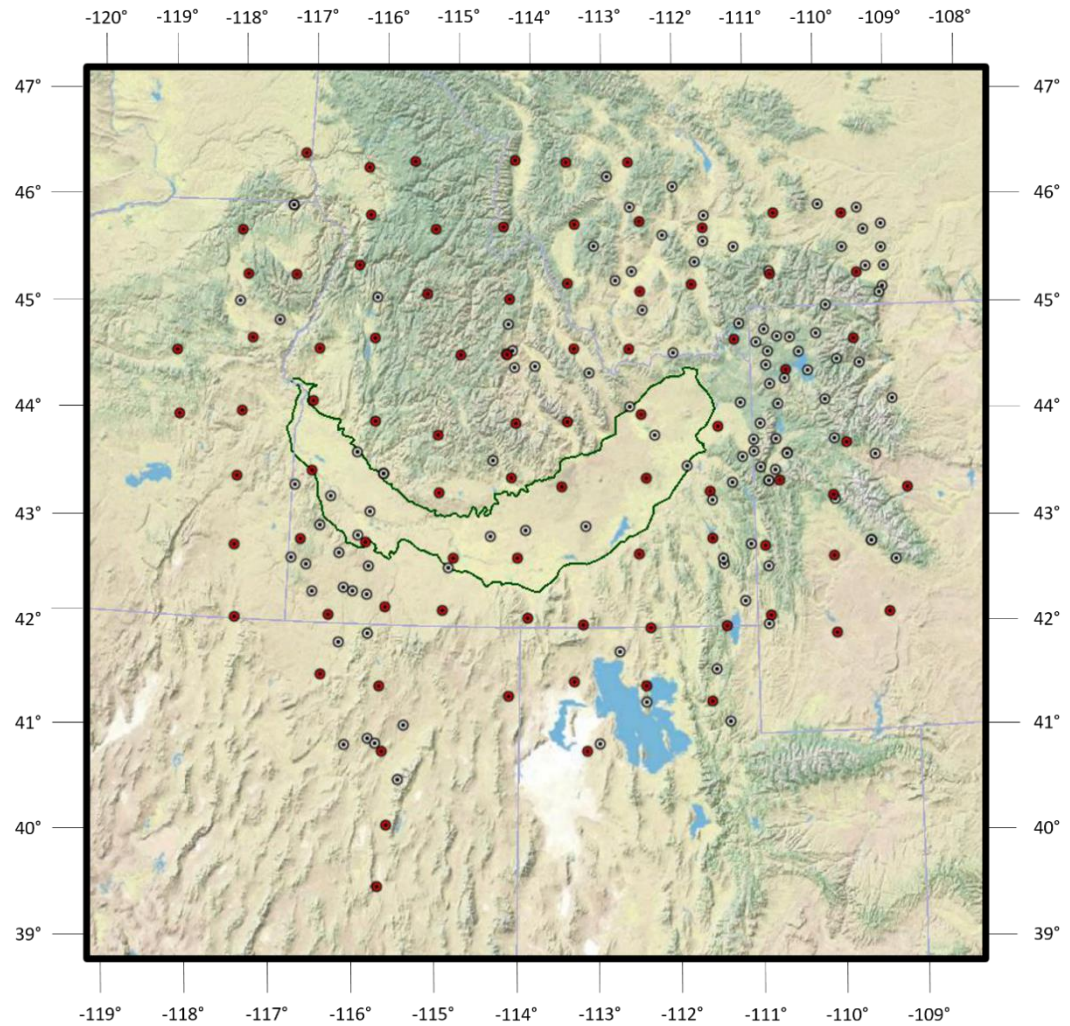
Figure 9.   **A map showing the seismic stations (bullseyes) used in this study. USArray stations are red while stations from other various studies are white. The topographic expression of the SRP is outlined in green.**

A majority of the seismic data was obtained through Earthscope Automated Receiver Survey (EARS). EARS is a EarthScope/USArray data product that uses an automatic receiver function generator (Crotwell and Owens, 2005) to estimate the crustal thickness and Vp/Vs ratio across the continental United States. This project utilizes earthquakes above magnitude 5.5 and between 30 and 100-degree great circle distance from all broadband, three component seismic stations available from IRIS DMC. The

data is available at http://ds.iris.edu/ds/products/ears/. The automatic receiver function generator uses the iterative deconvolution technique of Ligorria and Ammon (1999) with a Gaussian width of 2.5, producing both radial and transverse receiver functions. See Crotwell and Owens (2005) for more information on the processing of the EARS receiver functions.

Additional seismic data from seismographs in my study area were available at the IRIS DMC that were not on the EARS database. This includes data from the HLP (James and Fouch, 2006) and Ruby Mountains core complex experiment (Klemperer and Miller, 2010). To gather and produce receiver functions of this data, I used the MATLAB toolbox, FuncLab (Porritt and Miller, 2018). FuncLab is a data management system with tools to produce, manage, and visualize receiver function data.

All of the earthquake events extracted from FuncLab were above a 5.5 magnitude, and originated from a great circle distance of 30-100 degrees between the years 2006-2012. The original seismic data contained 120 seconds of three-component seismic information at a sample rate of 40 Hz, starting 30 seconds before the first (P-wave) arrival. The data were preprocessed using a 5% taper to the start and end, and a bandpass filter between 0.02 and 5 Hz. The iterative deconvolution technique of Ligorria and Ammon (1999) was then applied, using a Gaussian width of 2.5 with 400 as the maximum number of iterations and a minimum error of 0.0001 s. These steps are very similar to the steps used by EARS (Crotwell and Owens, 2005) and when comparing results, produce nearly identical waveforms.

To infill the IRIS and affiliate data, three seismic stations were used from the Fort Boise Noise observation (Xu, personal comm.). These data were collected in the city of

Boise, Idaho using three 250 Hz broadband seismometers that were located within 200 meters of each other. To extract the seismic waveforms, I looked for seismic signatures of teleseismic earthquakes above a 5.5 magnitude that originated from a distance of 30-100 degrees. The raw data were then bandpass filtered between 0.3 and 1.5 Hz. For seismic events that were visible on more than one station, the data was stacked to help remove noise present within the data. The radial and vertical components of the seismic data were then used to produce a receiver function using the deconvolution method of Ligorria and Ammon (1999). Overall, 22 seismic events were produced into a receiver function waveform. Comparable results from this station when compared to published station data shows the robustness of this approach to extract velocity structure within the crust.

Metropolis Algorithm Inversion Technique

In order to accurately convert these receiver function waveforms into an Earth velocity model, I utilize an inversion scheme. This inversion must construct Earth model parameters that, when forward modelled, will output receiver function data that match the observed receiver function data while minimizing the travel time shift. This can be a challenging problem because in general, the inversion of receiver functions is highly non-linear and non-unique. In order to avoid these problems, the number of parameters must be limited. For my analysis, I varied only two parameters, depth to layers and the P-wave velocity of these layers. The assumptions made to minimize the non-linearity and non-uniqueness of the inversion include holding the Vp/Vs ratio constant at 1.73, assuming the Earth behaves as a Poisson solid (Shearer, 1999), and holding the density constant following the Birch law (Birch, 1964):

$$\rho \left(\frac{kg}{m^3}\right) = 0.32 \left(\frac{kg*s}{m^3*km}\right) * Vp \left(\frac{km}{s}\right) + 770 \left(\frac{km}{m^3}\right)$$

While these assumptions help minimize the non-linearity and non-uniqueness of the inversion, they also introduce more error. It is very unlikely that the Earth would have a constant Vp/Vs ratio and density, and therefore, amplitude and travel time errors are present in my results.

I also constrain the P-wave velocities within realistic bounds, based on the seismic velocities of Christensen and Mooney (1995). These velocities are featured in Figure 10 below.
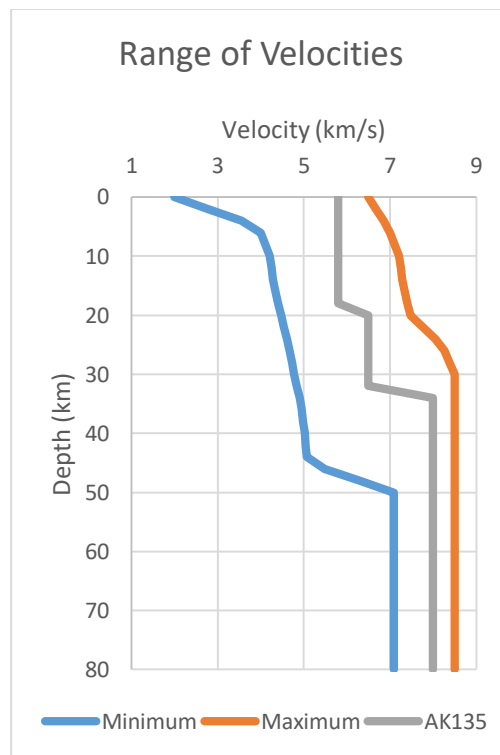
Figure 10. **Plot showing the velocity constraints for my inversion approach. The blue line represents the minimum velocity and the orange represents the maximum velocity that I accept in my model. Velocity limits were based on Christensen and Mooney (1995). The gray line represents the AK135 standard Earth model and is the starting model for my inversions.**

The forward modeling technique that I use is modified MATLAB code that generates synthetic seismograms from a given Earth model (Jacobsen and Svenningsen, 2008). Once a synthetic seismogram is calculated, a bandpass filter is applied to match

the observed data. A deconvolution between the vertical and radial component is then calculated using the iterative deconvolution technique of Ligorria and Ammon (1999), using the same parameters as above, giving the final receiver function waveform.

The inversion technique used in this project is the Metropolis algorithm, which is based on the work by Jansson (2008). This method is considered a Markov Chain Monte Carlo method, which is a sequence of random models that depend only on the previous model. For more information on the Metropolis algorithm, see Mosegaard and Sambridge (2002).

The process of the Metropolis algorithm can best be described in six steps:

(1) Start with a simple Earth model. The starting model is extremely important due to the non-uniqueness present in the inversion of receiver functions. Here, I use 2-km thick layers with velocities matching the standard AK135 Earth model (Kennett et al., 1995; Figure 10) with an adjusted Moho depth derived from previous studies that include the EARS database (Crotwell and Owens, 2005), Eager (2010), and Litherland and Klemperer (2017). The selection of a 2-km layer thickness will be discussed in further detail in chapter 3.

(2) Adjust a random two km thick layer's velocity by a random amount. This fluctuation in velocity is held to less than 0.5 km/s and the velocities remain within the bounds shown in Figure 10.

(3) Generate the receiver function for the new Earth model via forward modeling.

(4) Calculate the root-mean-square (RMS) error misfit between the observed and synthetic receiver function. RMS error is a standard method of calculating the misfit

between two sets of data. For this inversion, the units of RMS will be ignored because each waveform is normalized to an amplitude of 0.6.

(5) If the misfit of the new model is less than the previous iteration, the new model is accepted and you return to step 2.

(6) If the misfit of the new model is more than the previous, the new model is accepted with a probability of $\exp(-\frac{\Delta misfit}{s^2})$ and then return to step 2. This function is also referred to as the "Metropolis rule" and helps the inversion jump out of any local minima (Metropolis et al., 1953; Mosegaard and Tarantola, 1995; Jansson, 2008). Δmisfit is the change in misfit from the previous iteration to the current iteration. s^2 is the total "noise" variance and has a value of 0.1 for all inversions. Jansson (2008) determined this value to be a reasonable estimate for this inversion technique.

One of the challenges in Monte Carlo inversion techniques is to find a balance between exploration and exploitation. Exploration in this case, means to find the local minima and exploitation means to explore these local minima. Exploitation is covered by accepting the new model when the misfit decreases and exploration is covered by accepting the new model when the misfit increases. This means that exploration is controlled by the Metropolis rule.

CHAPTER THREE: RECEIVER FUNCTION INVERSION RESULTS

Receiver Function Signals

As shown in the DNA13 velocity perturbation images (Figure 4), I identify velocity anomalies in the crust that are likely related to changing temperature or lithology. While crustal velocity distributions were not the focus of the Porritt et al. (2014) study, other studies including Peng and Humphreys (1998), Eager et al. (2011) and Stanciu et al. (2016) have used receiver functions to identify partial melt and changing lithology in Idaho.

Within the receiver function waveform, differences in amplitude or phase represent changes in crustal velocities. This assumes ray paths are vertical and that noise is not a factor. In Figure 11a, the waveform for a homogeneous crust is shown with P, Ps, PpPs, and PsPs+PpPs arrivals (see Figure 8 arrival ray paths). Although these arrivals are usually prominent in receiver function waveforms, additional signals produced from reflected arrivals within the crust are often observed. Figure 11b shows the two-layer crust of the AK135 Earth model. Note the addition of peaks at about 3 and 9 seconds after the first arrival and a trough at about 12 seconds. These additional returns represent P-S converted waves from the added layer. In figure 11c, I show a stacked receiver function from the eastern Idaho station TA.K11A (see Figure 13a), where a positive amplitude return is observed at 1.5 s after the first arrival, and amplitude reversals are noted at about 3 and 7.5 seconds. This stacked waveform is produced by averaging 33 receiver functions from different earthquakes. Through forward modeling, this travel time

and amplitude pattern can be explained by a slow velocity lower crustal layer (Figure 11d). Note the variation in travel time and amplitude for individual receiver functions (Figure 11e). These variations are related to a violation in my assumption of vertically travelling earthquake travel paths or noise included on the seismogram. The variation velocity with respect to differing travel paths are discussed below.
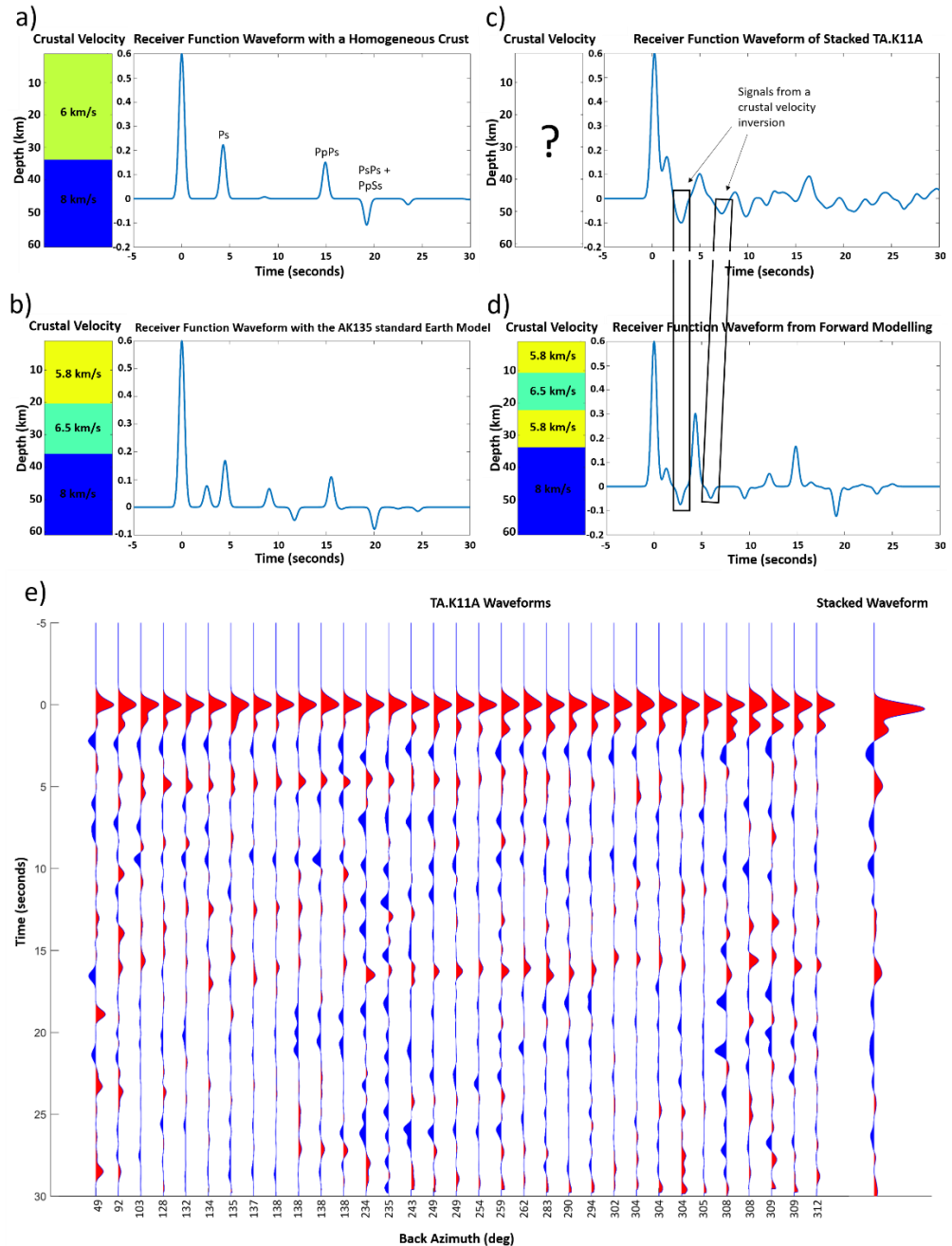
Figure 11. **a) A modeled receiver function for a single velocity crust and mantle. b) A modelled receiver function for the AK135 standard Earth model that contains two crustal layers and a 36 km thick crust. c) The stacked receiver function waveform for all earthquakes recorded on station TA.K11A. d) A modelled receiver function for a crustal model that consists of a 10 km thick low velocity zone above the 36 km deep Moho. e) All waveforms for station TA.K11A and the stacked waveform shown in figure 11c.**

Metropolis Algorithm Sensitivity Tests

To achieve a more accurate velocity model from receiver function waveforms, I utilize the Metropolis algorithm inversion technique. To test this approach, I use synthetic data that consists of a homogeneous crust to test the accuracy of the inversion (Figure 12). I use a crustal velocity of 6 km/s, a mantle velocity of 8 km/s, and a crustal thickness of 30 km. The starting model for the inversion in Figure 12a consists of a constant 7 km/s crust and mantle. After about 100 iterations, the Metropolis algorithm fits a velocity change at 34 km depth that closely matches the observed data, however, crustal thickness and crustal velocity is overestimated. In the bottom figure, I show the same receiver function, but I start my inversion with the AK135 standard Earth model with a crustal thickness of 34 km. With this starting model, the algorithm converges to more accurate velocities and crustal thickness. This exemplifies the fact that the starting model is very important in these inversions. For my inversions, I use the AK135 standard Earth model with crustal thickness estimates beneath each station as a further constraint. These H-k derived estimates come from the EARS database (Crotwell and Owens, 2005), Eager (2010), and Litherland and Klemperer (2017).
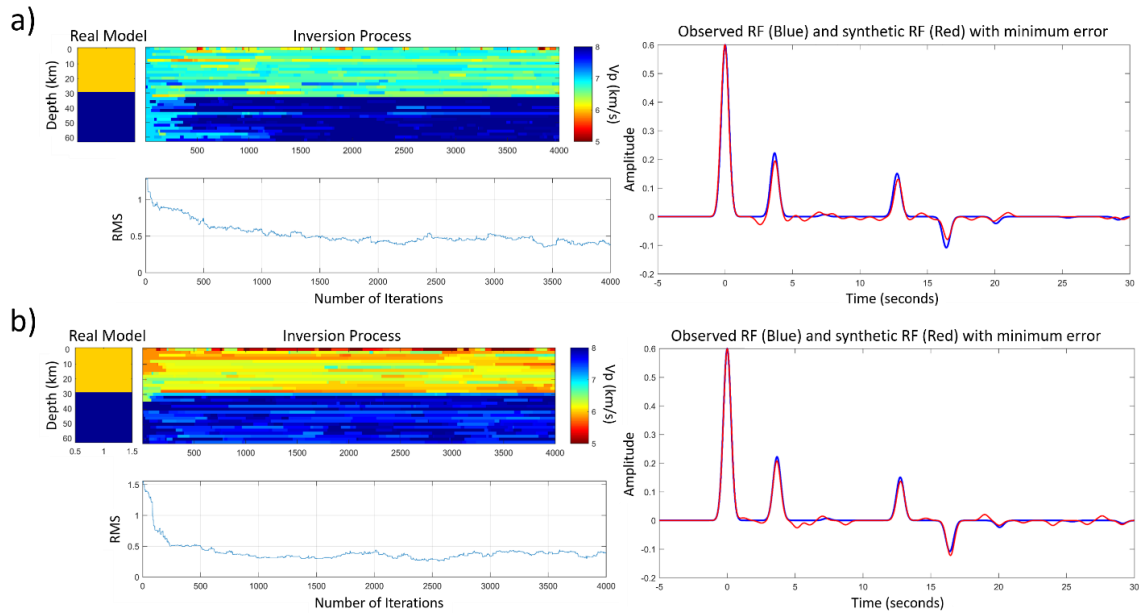
Figure 12. **Metropolis algorithm inversion applied to a synthetic waveform generated by a single layered crust (leftmost figure). The observed/known receiver function waveform is in blue while the synthetic/calculated receiver function waveform is in red (rightmost figures). a) The starting model for the inversion is a constant 7 km/s and converges to a solution that overestimates the Moho depth and crustal velocity. b) The starting model is the AK135 standard Earth model where my inversion converges to a solution that more accurately reflects the true model with fewer iterations.**

To explore the range of crustal velocities beneath Idaho, I select three stations with contrasting crustal lithologies; TA.I12A, located on rocks associated with the granitic Idaho Batholith; XC.Y03, located on basaltic rocks of the eastern SRP; and TA.K11A, located along the southern margin of the western SRP (Figure 13a).

Presumably, the Idaho Batholith contains a simpler crustal velocity distribution when compared to a station from eastern Idaho due to the presence of intrusive rocks along the path of the Yellowstone hot spot (e.g., Stanciu et al., 2016; Peng and Humphreys, 1998). In Figure 13b, I show an observed waveform from station TA.I12A and the calculated waveform with minimal error. The crustal velocities for my calculated receiver function are similar to that of Davenport et al. (2017), showing a gradual

increase in velocity from the surface to the Moho, at 26 km depth. Stanciu et al. (2016) estimated the Moho for the Batholith to be at 34 km depth. This discrepancy could be because my station is roughly 80 km from their closest seismometers. The EARS database, derived from H-k analysis, lists the Moho for this station location to be 27 km.

Station XC.Y03 lies in the eastern SRP and, given basaltic layering, contains a more complex crustal structure than a station that lies upon the Idaho Batholith. High velocity mid-crustal sills have been imaged in this region using a variety of geophysical methods (Priestley and Orcutt, 1982; Sparlin et al., 1982; Peng and Humphreys (1998); Stachnik et al. 2008). In my inversion result (Figure 13c), I identify a high velocity zone 8-12 km deep that could represent a cooled sill complex. The depth to the top of this sill is consistent with observations made by Priestley and Orcutt (1982), Sparlin et al. (1982), and Peng and Humphreys (1998), but my sill is approximately 6 km thinner. The Moho is also much deeper here (~44 km depth), consistent with the EARS database, Peng and Humphreys (1998), and Yuan et al. (2010).

Station TA.K11A is located in southwest Idaho, and is close to where I note a low velocity crustal anomaly in the DNA13 dataset (Figure 4). Figure 13d shows my inversion results for this station, containing a low velocity inversion at 20-30 km depth, which is similar to the DNA13 dataset. Here, my model shows a crustal thickness of 40 km, similar to the Eagar et al. (2011) results of ~38 km and EARS published H-k derived depth of 38 km.

In summary, where previous studies have focused on crustal velocities of the Idaho batholith, and portions of the SRP, my modeling approach shows consistent results.

Because my analysis spans these focus areas, I highlight changes in crustal properties across multiple geologic provinces.
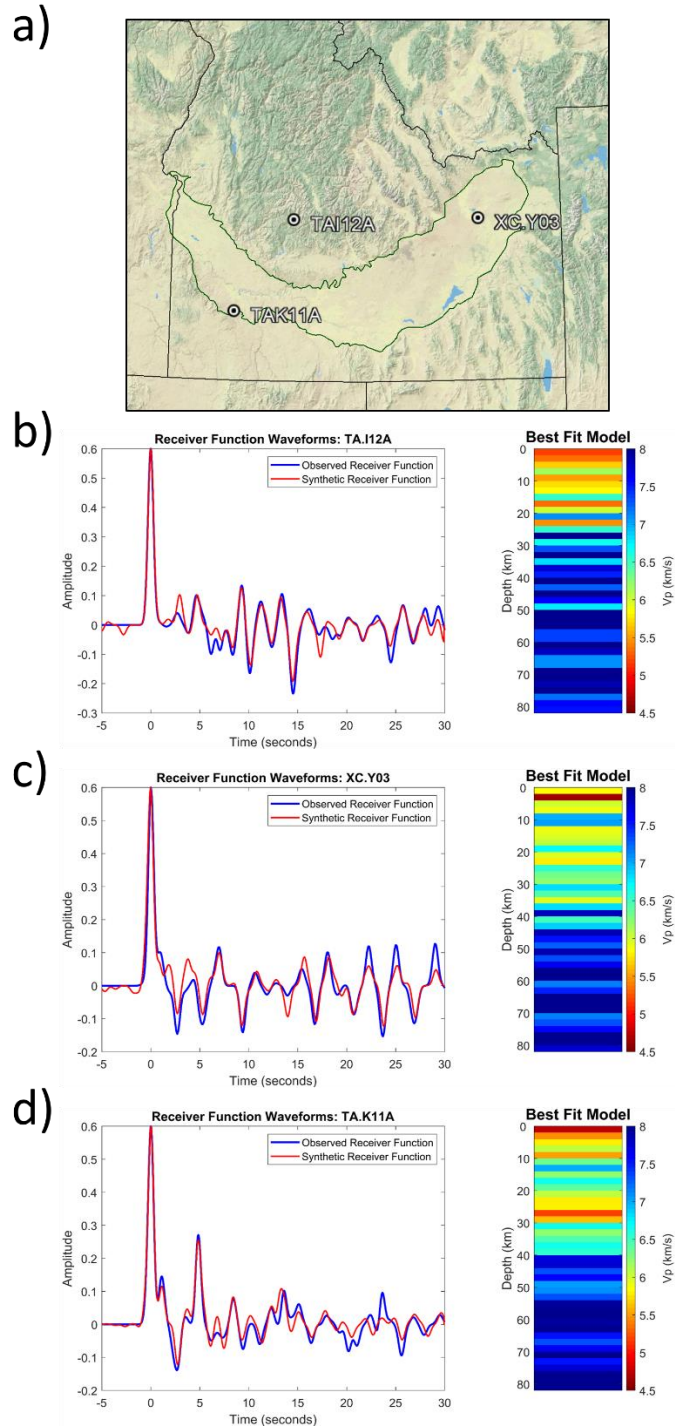
Figure 13. **Examples of the receiver function inversion where the difference in observed/known receiver function waveform (blue) and synthetic/calculated**

**receiver function waveform (red) of figures b, c, and d are minimized. a) A map
showing the station locations for the example inversions. The topographic
expression of the SRP is outlined in green. Inversion and calculated waveforms for
b) an event at station TA.I12A located in the Idaho batholith. c) an event at station
XC.Y03 located in the eastern SRP. d) an event at station TA.K11A located in the
southern margin of the western SRP.**

The selection of a 2-km layer thickness was chosen for five reasons related to
optimization of the inversion calculation and seismic resolution of the input dataset. The
reasons are: (1) The motivation of this study was to identify mid and lower-crustal
features rather than bulk crustal properties, so a relatively small layer thickness is better.
(2) Signals produced from layers under 2 km thickness would be poorly resolved.
Assuming an average crustal velocity of 6 km/s and the highest signal frequency of 3 Hz,
we obtain an average wavelength of 2 km. (3) The computation required to forward
model the receiver function for 1 km layers is nearly doubled compared to 2 km layers.
(4) The difference in RMS error between the 1 km layer and 2 km layer model is
negligible (Figure 14a and 14b). (5) A layer thickness larger than 2-km provides much
larger RMS errors (Figure 14c and 14d). Thus, a 2 km layer thickness provides a balance
between resolution and computation time where a typical crustal thickness of 40 km
provides a 20-layer model; adequate to identify and characterize anomalous regional
crustal velocities.
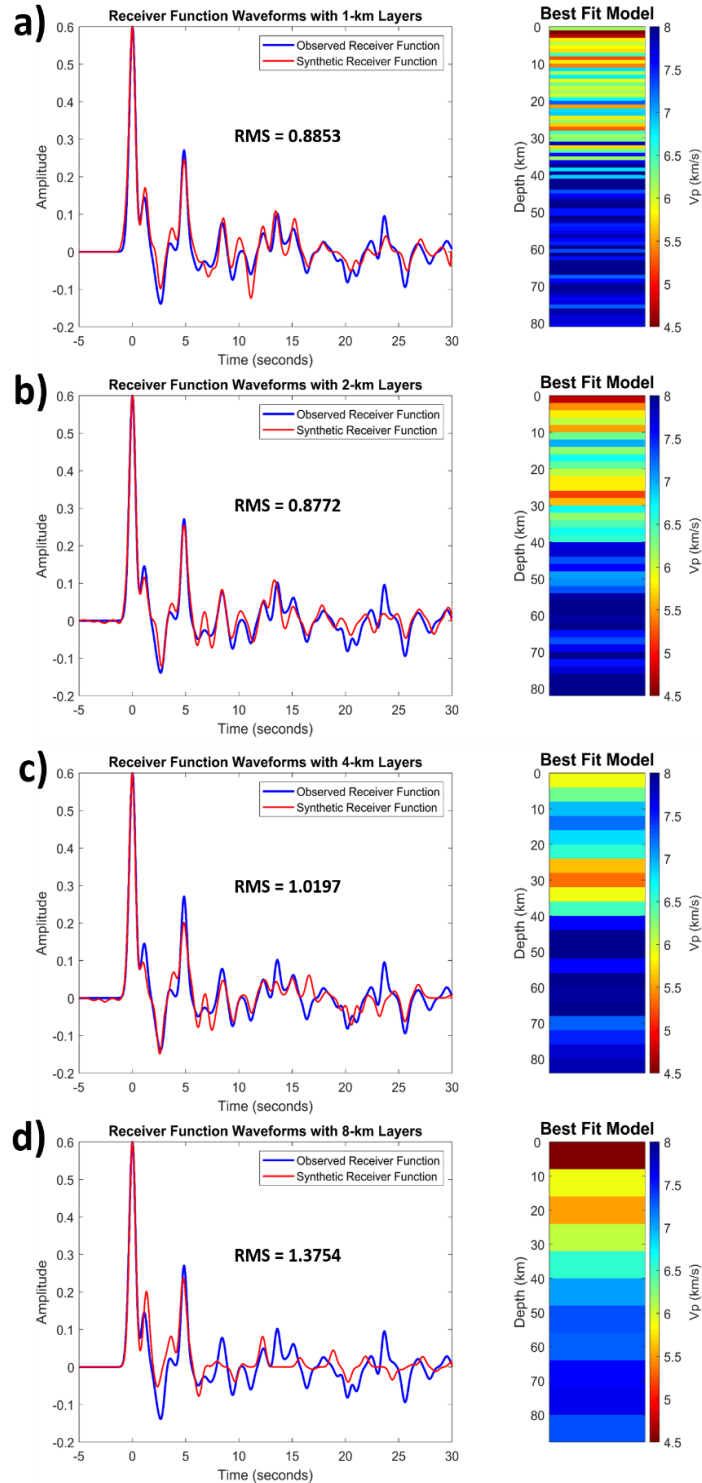
Figure 14. **Examples of receiver functions waveforms with different layer thicknesses to test layer thickness sensitivities. The observed/known receiver function waveform is in blue while the synthetic/calculated receiver function waveform is in red. Figure a, b, c, and d have layer thicknesses of 1, 2, 4, and 8 km respectively.**

Tomogram Constructions

I inverted 14107 earthquake records from 202 stations across southern Idaho and surrounding areas. To eliminate outliers from noisy or poorly constrained data, I accept the 1-D velocity model only if the RMS error is below 1.5, resulting in 8725 usable velocity models (see Yang et al., 2016). This error threshold is based on a qualitative comparison of the observed and synthetic receiver function. Figure 15 shows this comparison to the same earthquake event used in Figures 13d and 14. An RMS error above 1.5 (Figures 15a and 15b) fails to match many of the signals, while an RMS error at or below 1.5 (Figures 15c and 15d) have more comparable signals. Figure 16 shows the RMS error for all receiver functions. Once each receiver function is inverted and a 1-D seismic velocity model is achieved, these models are put together to create a 3-D tomogram.
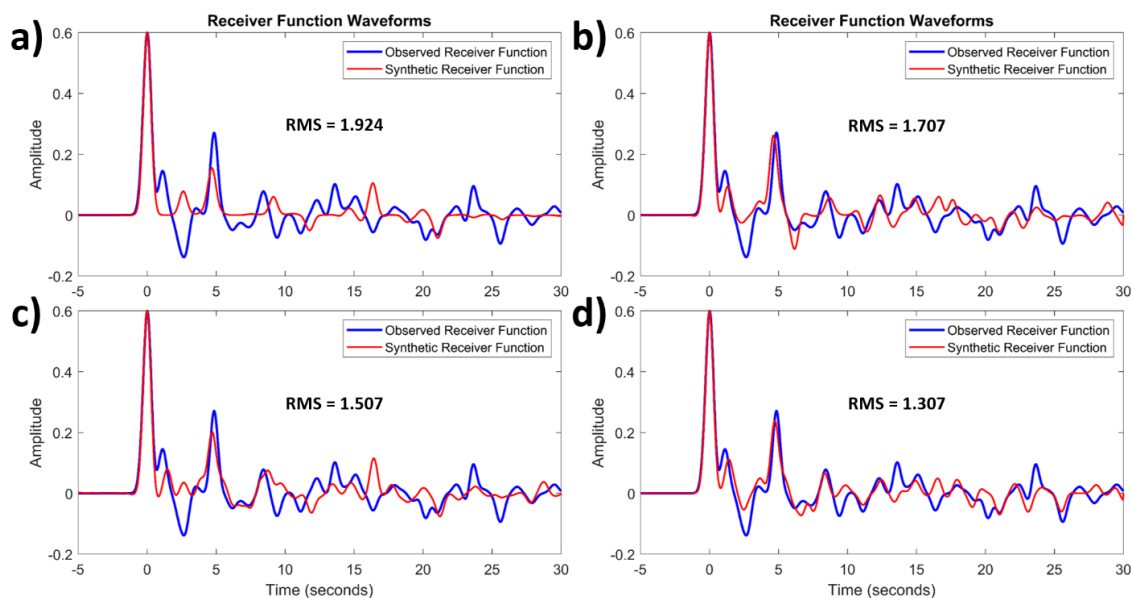
Figure 15.   Examples of receiver functions waveforms with different RMS values. The observed/known receiver function waveform is in blue while the synthetic/calculated receiver function waveform is in red. Figure a, b, c, and d have RMS values of 1.924, 1.707, 1.507, and 1.307 respectively.
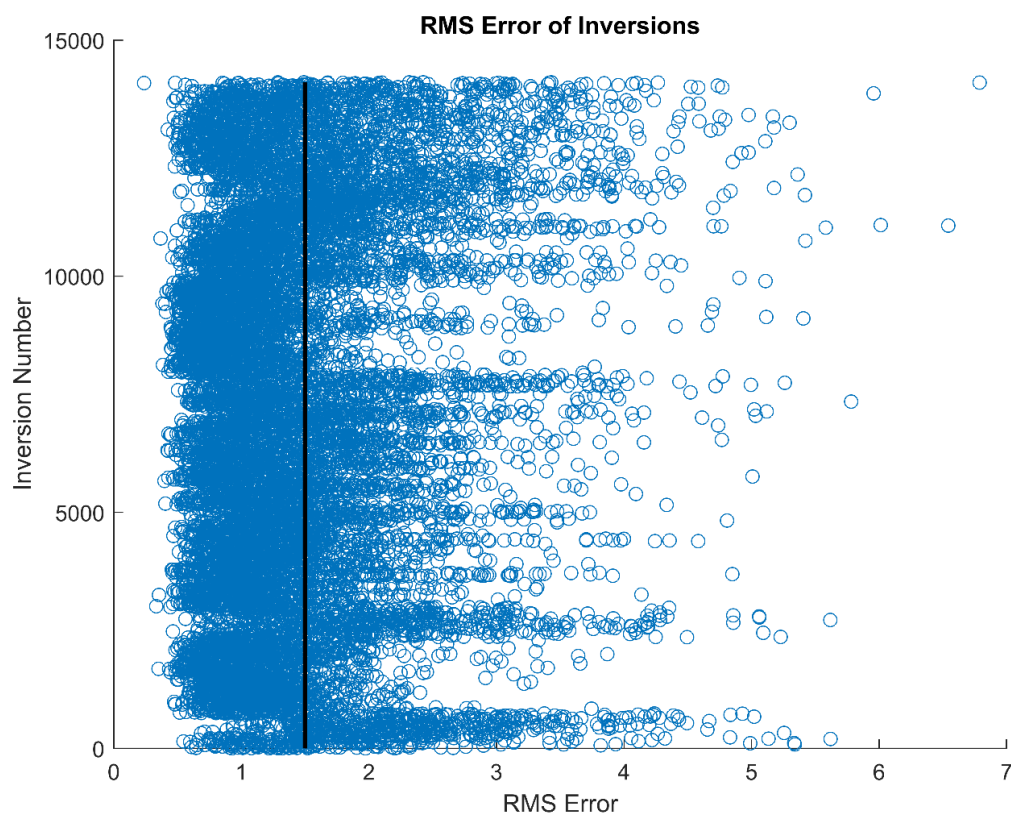
Figure 16.   The RMS error for all 14107 events. If the RMS error exceeded 1.5 (black vertical line), the crustal model from the inversion was not used.

To construct a 3-D tomogram, I first estimate the travel path and ray piercing points for a given depth using 1-D ray tracing. Because each earthquake travels along a different path that depends on epicentral distance and azimuth, each earthquake for a station may contain different amplitude and travel time information that can be used for building a 3-D model. This is similar to common conversion point stacking for receiver functions (Dueker and Sheehan, 1997) or common midpoint stacking for reflection processing (Yilmaz, 2001). Because events from a closer epicentral distance arrive at a shallower emergence angle, the piercing point at 60 km depth is located upwards of 30 km lateral distance away from the station. This results in velocities being best constrained at greater depths, whereas at shallow depths, velocities can only be constrained directly

beneath the station location. This also explains some variations in receiver function waveforms for different earthquakes (Figure 11).

Once the piercing point coordinate is calculated for each depth, the corresponding velocity for each receiver function is binned to a 2x2x2 km grid. Topography is also accounted for in this process by simply adding the station elevation to the depth measurements prior to binning. I select a 2D linear interpolation scheme based on an average of the 8 nearest neighbors to infill each empty cell within each layer. Once every depth layer is interpolated, I merge each layer to form a 3-D model. I then smooth this volume using a 6x6x6 km box filter. This filter was chosen because of its ability to remove irregular velocities within the 3D volume, and it produced the most realistic results when compared to other box filters. It should be noted that calculated velocities that are a significant distance from a recording station are poorly resolved.

CHAPTER FOUR: RESULTS AND DISCUSSION

Crustal Thickness Variations

To estimate crustal thickness, I identify the depth to the 7.2 km/s contour within the 3D model. This velocity value is found in the transition from an average lower crustal velocity (6.5 km/s) to an average upper mantle velocity (8.04 km/s) based on the AK135 standard Earth model (Kennett et al., 1995). This transition value is also consistent with lithology/velocity estimates from DeNosaquo et al (2009) (Figure 6). This assumption results in a crustal thickness range of 25-45 km depth across my study area (Figure 17) and is consistent with many other focused studies. The thinnest crust is associated with the region surrounding the Oregon-Idaho graben and with the Basin and Range province beneath northwest Utah. The thin crust beneath the Oregon-Idaho graben region has been attributed to Miocene and younger extension (Cummings et al., 2000). Similar processes are at play along the eastern limits of the Basin and Range in northwest Utah (Latitude: 41, Longitude: -113).

The transition from thin to thick crust south of southeastern Idaho (Figure 17) corresponds to the transition from the Basin and Range province to the Middle Rocky Mountains province across the Wasatch fault (Figure 1). In a seismic refraction experiment by Braile et al. (1974), a 28 km thick crust was determined beneath the Basin and Range province while a 40 km thick crust was found in the Middle Rocky Mountains farther east. These measurements are consistent with the shallow to deep Moho transition in northern Utah from my receiver function analyses.

The crustal thickness beneath the Idaho Batholith is roughly ~30 km deep and is separated from the Basin and Range province to the east, with a Moho depth of ~35 km. Crustal thickness across the WISZ does not appear to change as observed in the studies by Stanciu et al. (2016) and Davenport et al. (2017). This is likely due to the lack of station coverage compared to the studies that have worked on this problem. There is no clear transition between the Idaho Batholith and its surrounding regions. Although there are some stations in the HLP and CRB provinces, there is not enough station coverage to make any interpretations about crustal thickness geometry.

Along the past 14 Ma track of the Yellowstone hotspot, I observe a 5-10 km increase in crustal thickness compared to adjacent regions. The width of this anomalous zone is consistent with the topographic expression of the eastern SRP and extends back toward the region of hot spot initiation (Figure 17). Yuan et al. (2010) suggested that these changes are a result of additional mass from crustal magmatic injections. The crustal thickness is also greatest beneath the youngest portion of the eastern SRP (45 km) and appears to gradually decrease in thickness towards the southwest (38 km). These observations are consistent with active and passive seismic studies of Yuan et al. (2010) and Eager et al. (2011). However, DeNosaquo et al. (2009) did not show increasing crustal thicknesses along the hot spot track and attribute measured differences to higher density mid crustal sills beneath the central portions of the SRP.
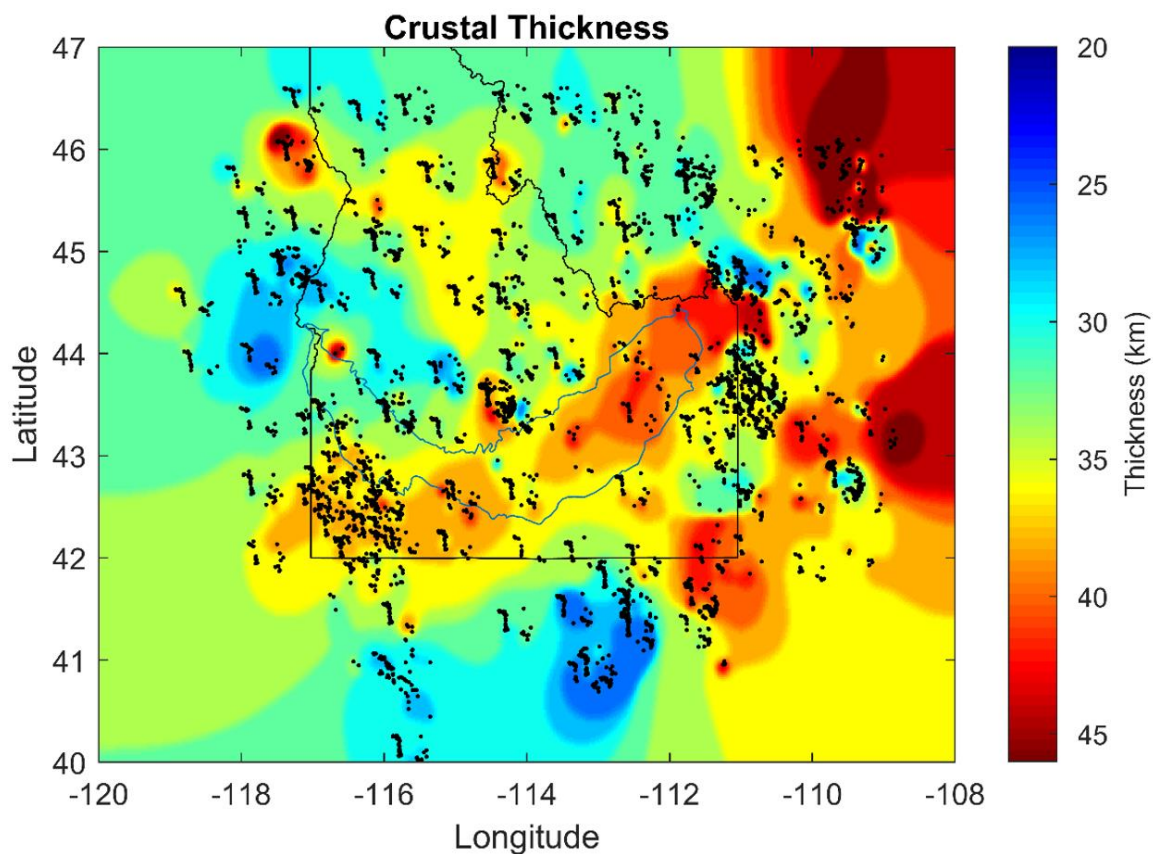
Figure 17. **Map of crustal thickness from receiver function inversions. Dots represent the piercing point at the average Moho depth for southern Idaho (36 km). The topographic expression of the SRP is outlined in green. Blue areas and red areas of indicative of a thinner and thicker crust, respectively.**

It appears that where caldera centers are mapped (Anders et al., 2014), there is a general increase in crustal thickness (Figure 18). This is most notable between the Twin Falls and Picabo eruptive center (purple star in the figure 18). Although only represented by a few seismic stations, the distribution of piercing points at these stations and at Moho depths support this observation (Figure 17). I observe a decrease in crustal thickness from ~41 km to ~36 km from the Picabo eruptive center to the zone between eruptive centers (purple star). The crust then thickens from ~36 km to ~39 km toward the Twin Falls eruptive center.

A relationship between crustal thickness and hotspot location as inferred from geodetic measurements is also observed. Anders et al. (2014) compared the distribution of eruptive centers with age to determine a North American plate velocity between 2.3 and 2.38 cm/yr for the last 10 Ma. With this plate rate, the hotspot location with age is plotted on Figure 18. This shows a zone of overthickened crust (~42 km average) extending back to 10 Ma. Before 10 Ma, Anders et al (2014) showed that the timing of eruptive centers does not correlate with a constant plate velocity. There are two ideas for this discrepancy: (1) plate rates need to be about 7 cm/yr before 10 Ma to match eruptive center ages with location (Pierce and Morgan, 1992) or (2) hotspot derived magma emplacement in the crust was more diffuse and therefore regions of overthickened crust do not match geodetic plate rates (Geist and Richards, 1993). While my crustal thickness measurements cannot provide insight as to which idea is correct, I do see a consistent pattern in crustal thickness post-10 Ma hotspot position compared to the pre-10 Ma crust; as the crustal thickening is more diffuse and is not as overthickened as the younger crust to the northeast. An alternative to either hypothesis is that my assumption of a 7.2 km/s transition from crust to mantle is not valid along the length of the hot spot track.
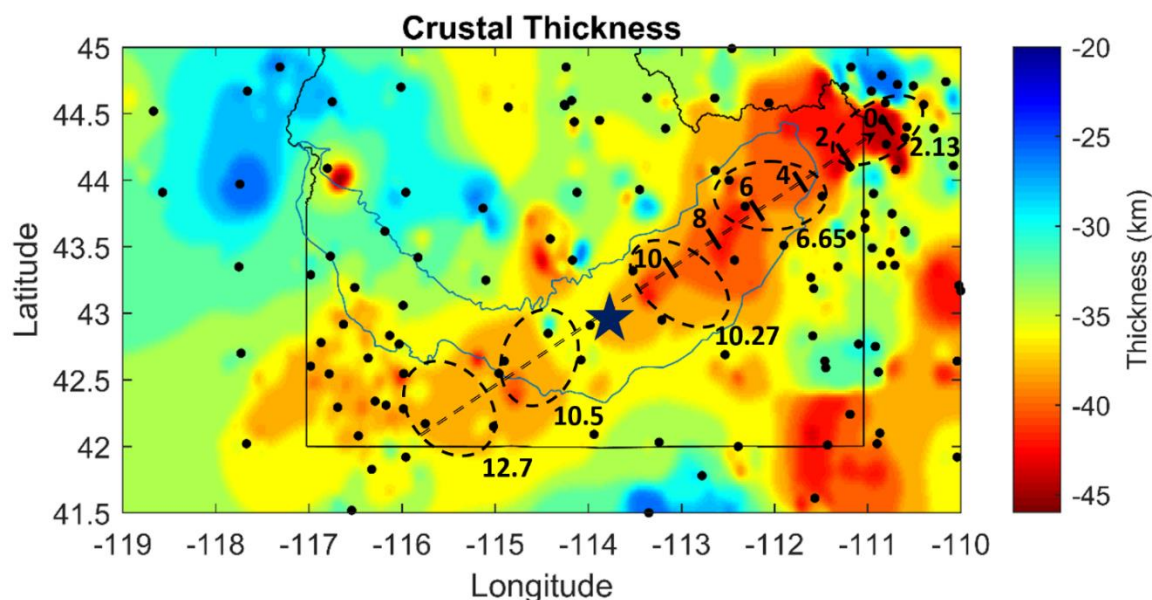
Figure 18. Map of crustal thickness from receiver function inversions. Numbers and hash marks represent hot spot geodetic position in Ma (from Anders et al., 2014). Dots represent the seismic station locations. The topographic expression of the SRP is outlined in green. Black dashed ovals are eruptive centers and their respective ages (from Anders et al., 2014). Black dashed linear line represents the track of the hotspot. The purple star represents an area of thinner crust that is located between eruptive centers.

Mid-Crustal Seismic Velocities: Distribution of Mafic Intrusive Rocks

In Figure 19, I average the velocities derived from my receiver function analyses between 6-14 km depth to obtain a map of mid-crustal seismic velocities. The most notable high velocity signal follows the track of the Yellowstone hotspot back to the 16 Ma hot spot origin near McDermitt, Nevada (Latitude: 42 Longitude: -117.7). These higher velocities when compared to surrounding regions is likely due to the replacement of ~6 km/s crust that is observed to the north and south of the SRP (e.g., Lerch et al., 2007; Davenport, 2016) with the emplacement of 6.2-6.4 km/s mid-crustal dioritic sills (Figure 6). This interpretation agrees with previous work regarding the presence of mid-crustal sills in the eastern SRP (Priestley and Orcutt, 1982; Sparlin et al., 1982; Peng and Humphreys, 1998; Stachnik et al. 2008; DeNosaquo et al, 2009). This observation also

suggests that although crustal thickness estimates suggest a more diffuse hot spot emplacement of volcanic materials in the lower crust, materials in the mid-crust were more consistent and focused back in time to hot spot initiation. Note that my 12-16 km depth slice does not show anomalously high seismic velocities in the McDermitt region.

Figure 19 also shows that the mid crust beneath the western SRP does not contain significant amounts of mafic materials and the velocities are more similar to Idaho Batholith rocks that are mapped to the north. At shallower depths (4-8 km), I note higher seismic velocities match the contour of the western SRP, consistent with basaltic rocks mapped in borehole and with gravity data. This supports an idea that narrow dikes and broad thin sills occupy the western SRP.

Another feature observed in Figure 19 is the high velocity zone located beneath the Weiser embayment (Latitude: 44 Longitude: -117; Figure 1). This anomaly is centered west of the WISZ and is therefore part of the Blue Mountains Province accreted terranes. Davenport et al. (2017) measured a velocity of ~6.4 km/s for the mid crust for this region, whereas east of the WISZ, Davenport et al. (2017) measured a velocity of ~6.2 km/s. This decrease in seismic velocity across the WISZ is consistent with my observations. These changes in velocity can be attributed to the more intermediate crust west of the WISZ where east of the WISZ is a more felsic crust. Other details regarding the crustal properties for this region are highlighted in Stanciu et al. (2016) and Davenport et al. (2017).

A NEN-SWS trending low velocity zone of 5.5 km/s coincides with the current location of the Yellowstone hotspot (Figure 19). A magma reservoir has been seismically imaged beneath Yellowstone by Smith et al. (2009) and Huang et al. (2015) from roughly

5-15 ±1 km depth, consistent with my observations. The Idaho Batholith and Basin and

Range province have a velocity of ~6.1 km/s and ~5.9 km/s respectively.
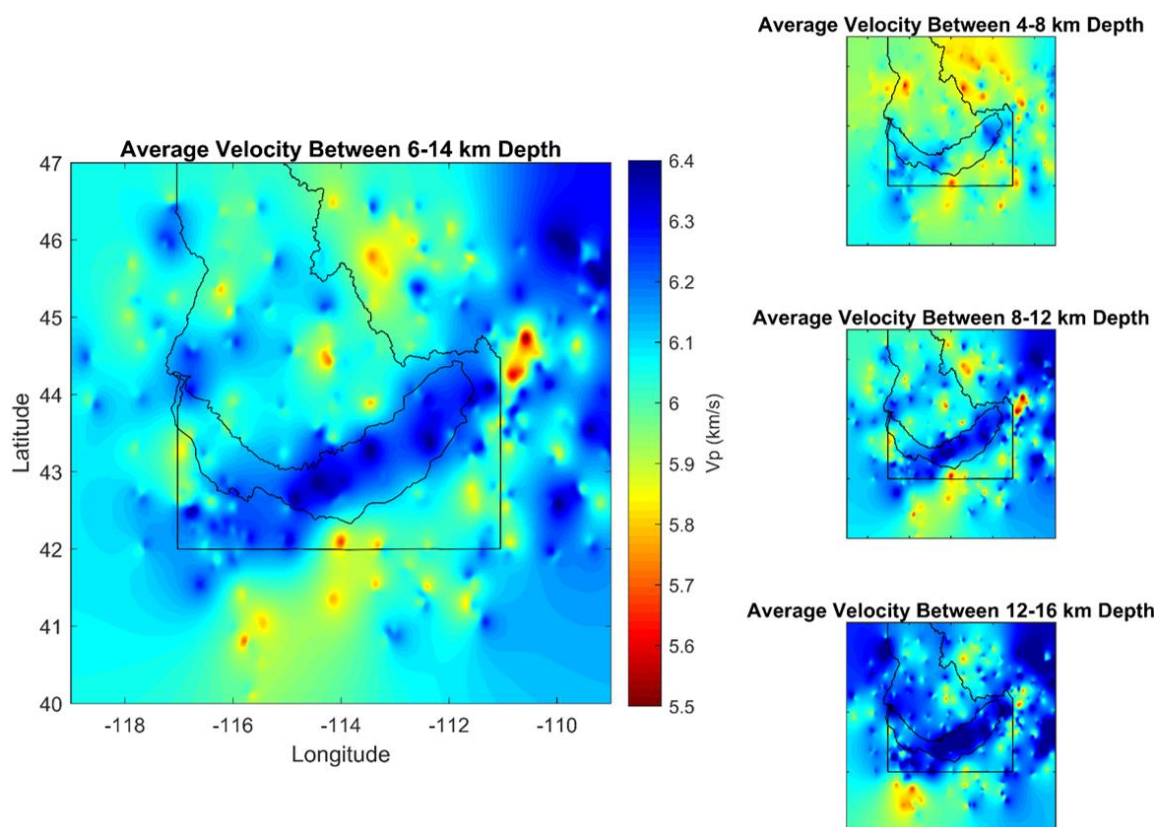
Figure 19. **Average velocities between 6-14, 4-8, 8-12, and 12-16 km depth. Both the topographic expression of the SRP and Idaho border are outlined in black. Blue areas and red areas of indicative of faster and slower velocities, respectively.**

Southern Idaho Cross Sections

To highlight seismic velocities across southern Idaho, I extract seven cross

sections from my final 3-D velocity model (Figure 20). I define the Moho where

velocities increase to greater than 7.2 km/s. Here, the gradient is consistently higher than

at other depths. This velocity contour increases in depth beneath the topographic

expression of the hotspot track (black vertical lines). Faster velocities are observed

between ~5-15 km depth beneath the hotspot track that I attribute to the presence of mid-crustal sills (Figure 19).

Whereas the results of my inversion generally produced smoothed lateral velocities in the lower crust, cross section B-B' shows narrow vertically oriented low velocity zones (6 km/s) in the lower crust beneath the southern margin of the western SRP. These low velocity zones are coincident with a high total magnetic field that has been interpreted to represent a narrow zone of mid-crustal dikes (Figure 3) (Glen and Ponce, 2002). Lastly, low velocities are seen at the base of the lower crust in line G-G' and the other cross sections beneath the topographic expression of the hotspot. Peng and Humphreys (1998) and DeNosaquo et al. (2009) made geologic interpretations that a thin layer of partial melt sits at the base of the crust of the eastern SRP.

Due to anonymously low velocities and history of volcanism, I suggest that the vertically oriented slow velocity zones beneath the southern margin of the western SRP may represent a zone of partial melt or differing lithology, and the horizontally oriented low velocity zones at the base of the crust under the eastern SRP are layers of partial melt. Although these velocities are not as slow as the 5.5 km/s shallow region beneath Yellowstone, where partial melt is identified, velocities in the range of 5.8-6 km/s at lower crustal depths could be of similar melt percentage due to the increase in pressure (DeNosaquo, 2009; Figure 6).

To address spatial resolution concerns regarding vertically oriented low velocity zones, I present Figure 21 that shows the location of piercing points that helped create the velocity profiles of B-B' and C-C'. The presence of raypaths at the same location of the anomalous velocities in B-B' show that these features have likely been created by lateral

variations in the velocity model. In line C-C', this same effect occurs but not to the same quantity as B-B', supporting the possibility of the presence of these intrusive bodies. Alternatively, these lateral changes in seismic velocity could be related to changing velocities out of the plane of the cross section. Structure that is observed in the velocity profile that does not have any corresponding piercing points is produced from interpolation of nearby piercing points.
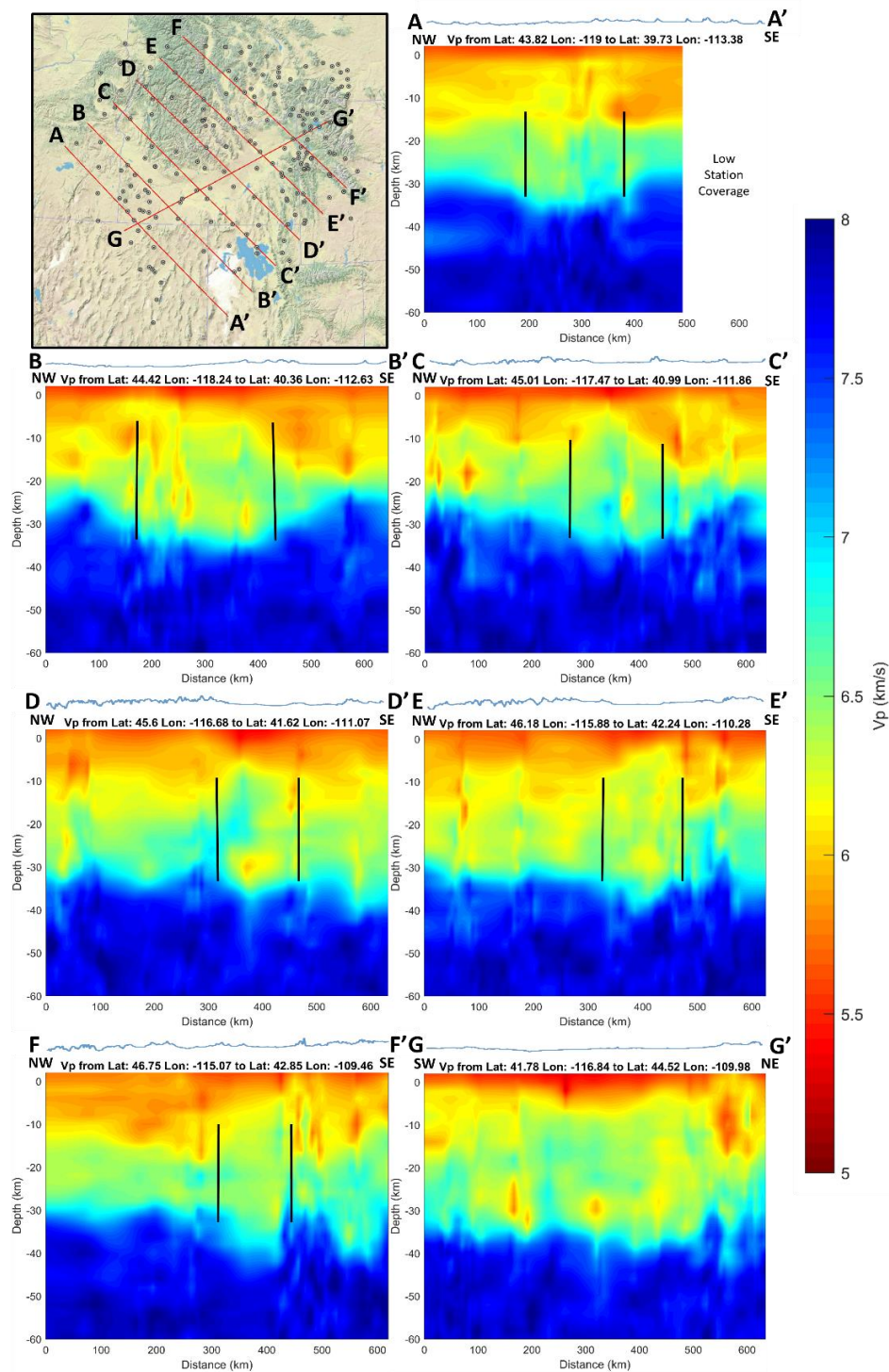
Figure 20. Top left: Map of the study area with red lines denoting the locations of the cross sections taken from the 3-D model generated from the receiver function inversions. Remaining figures: Velocity cross sections based on the inversion of receiver functions. The black vertical lines in cross sections A-F represent the area of deformation from the passage of the Yellowstone hotspot. Blue areas and red areas are indicative of faster and slower velocities, respectively.
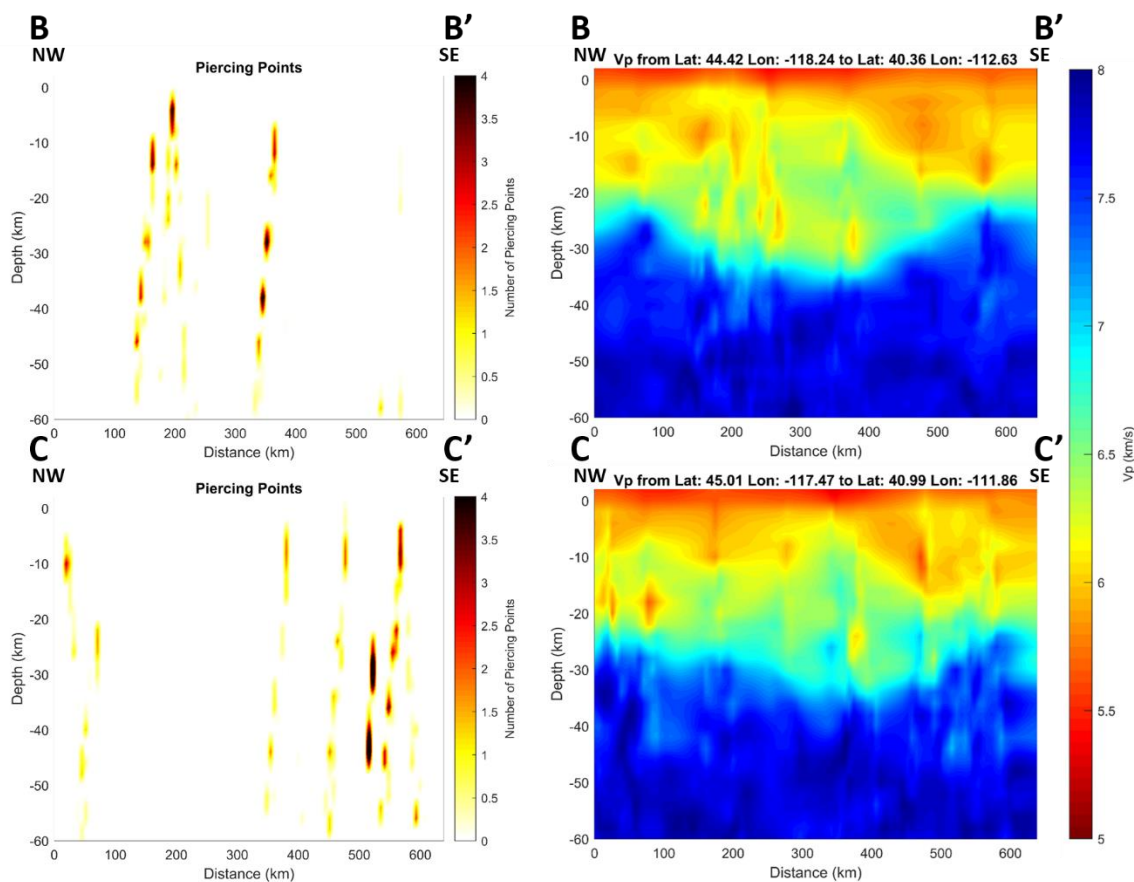
Figure 21. **Plots comparing piercing points (left) to the velocity profile (right). In line B-B', there are ray path piercing points that lead to anomalous velocity in the mid crust. In line C-C', this same effect occurs but not to the same quantity as B-B'.**

Tectonic Parabola

In figure 22, a relationship between seismicity

(https://earthquake.usgs.gov/earthquakes last accessed on August 2nd, 2018) and seismic

velocities derived from receiver functions is observed within what is called the "tectonic

parabola" (Anders et al., 1989). The tectonic parabola represents a zone of increased

seismicity centered on the Yellowstone hotspot, extending into eastern Idaho. Anders et

al. (1989) suggested that the seismicity pattern is created from reduced integrated

lithospheric strength produced by thermal effects of the hotspot. The aseismicity of the

eastern SRP is caused by the addition of mafic materials within the crust, increasing the

lithospheric strength. By comparing seismicity and upper crustal velocity, I see a positive correlation. Whereas almost no seismicity is observed where the velocity is greater than 6.2 km/s (except west to the Yellowstone caldera). the seismically active zones within the tectonic parabola shows consistently lower seismic velocities (denoted by A, B, and D in Figure 22). These slower regions tend to experience the most seismicity within the arms of the parabola. An area within the tectonic parabola that has a higher seismic velocity experiences almost no seismicity (denoted by C in Figure 22). These relationships offer evidence that this thermal weakening hypothesis is correct. Perhaps these areas are thermally heated, which in turn creates deformation and increases the local seismicity. This idea is consistent with observations of Smith and Sbar (1974) for portions of the tectonic parabola to the south of the eastern SRP. Alternatively, the low velocity zone at the border between Idaho, Utah and Nevada shows little to no seismicity, suggesting that additional analyses to explore this relationship is warranted.
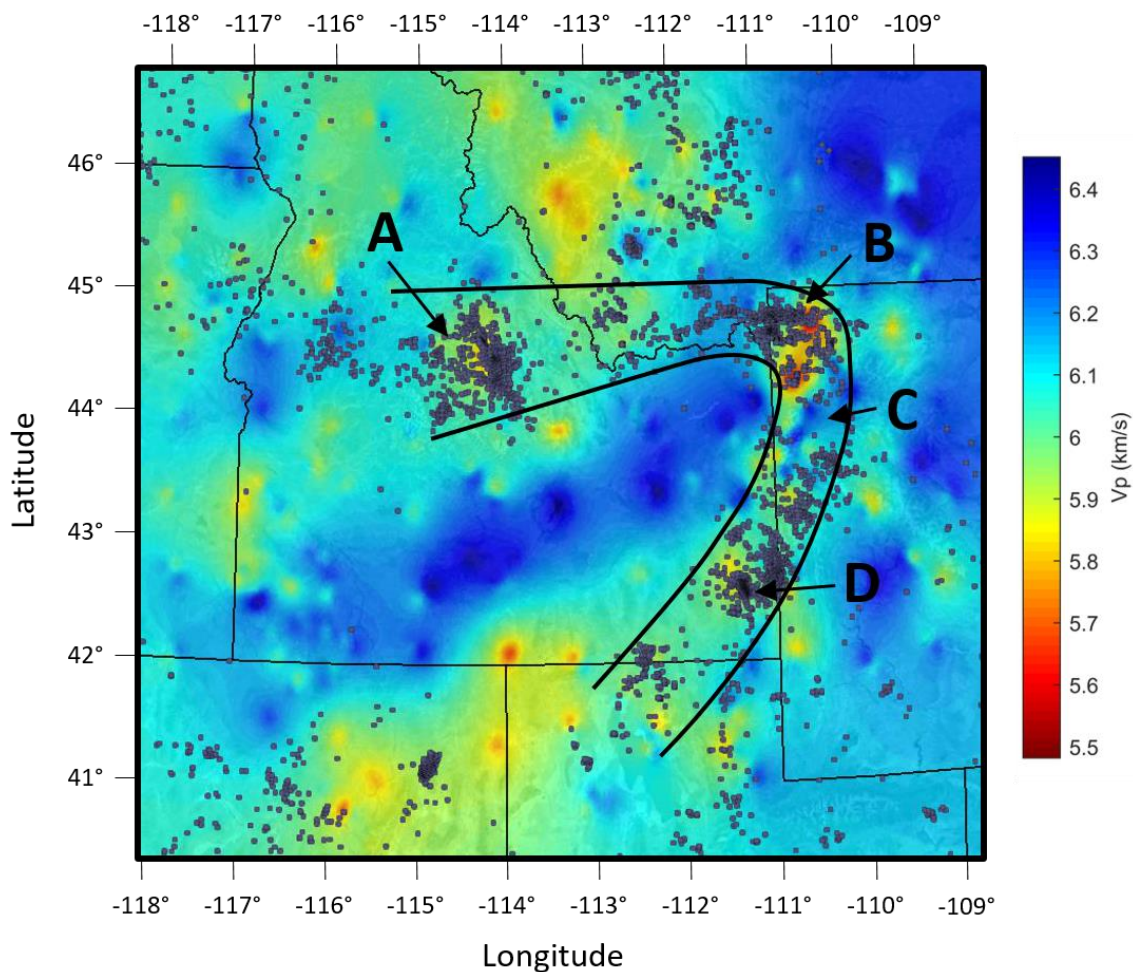
Figure 22. **The same as Figure 19, but with seismic events greater than magnitude 2.5 shown in gray dots. A relationship between seismicity and seismic velocity is observed where slower velocities correspond to more seismic events.**

Cross section sensitivities: Hill and Pakiser Inversion

To test the sensitivity of my velocity model, I compare a 1962 seismic refraction

survey that was performed using underground explosions over a 454 km line extending

from Eureka, Nevada to Boise, Idaho (Figure 2). The results were published by Hill and

Pakiser (1967) and then reinterpreted by Prodehl (1979), showing 1) a region of slower

velocity (~6 km/s) at 10 km depth below the western SRP, 2) a low velocity zone at 10-

20 km depth beneath the basin and range province of Nevada, and 3) crustal thickness ranging from 30-35 km depth (Figure 2).

Travel time data for the refraction survey is found in the Prodehl (1979) report. I use these travel time picks to invert for seismic velocity using the constraints of my receiver function results. Because seismic refraction models typically use an increasing velocity gradient as the starting model, and rays that encounter a velocity reversal often do not appear as first arrivals, it is difficult to resolve low velocity zones within the lower crust. Here, I will use the velocity model from the receiver function inversions as the starting model for the refraction inversion. The program used for these inversions was modified Matlab code from St. Clair (2015).

Figure 23a shows the profile extracted from my receiver function derived 3-D velocity model. I also show the calculated ray paths through this model from the St. Clair (2015) approach, and the travel times for those ray paths with the observed picks of Prodehl (1979). From this starting model, the RMS error is 0.93753 seconds. Although the travel time slope between observed and calculated arrivals are similar, the calculated arrivals are consistently early. After I run three inversion iterations, I achieve the model shown in Figures 23b. The RMS error is now at 0.61577 seconds and the calculated travel times are closer to the observed picks, with the exception of some outliers in the observed data.
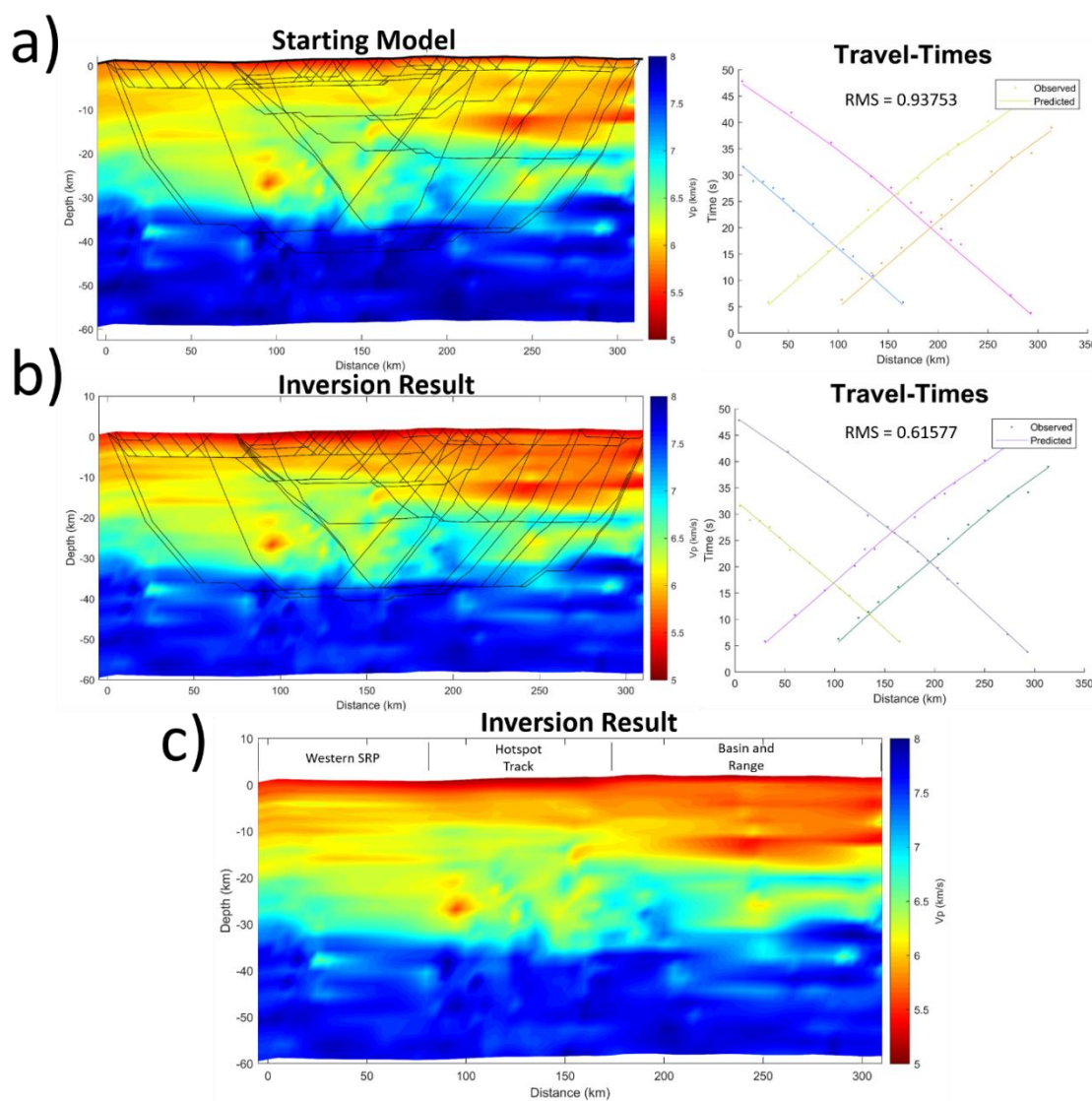
Figure 23. **Refraction inversion on Hill and Pakisers (1967) data using the receiver function results as the starting model. a) Left: The starting model for the refraction inversion with predicted ray paths. Right: The observed travel times (dots) and the predicted travel times for the starting model (lines). The RMS error is 0.93753. b) Left: The resulting velocity model after 3 inversion iterations with the predicted ray paths. Right: The observed travel times (dots) and the predicted travel times for the velocity model (lines). The RMS error is 0.61577. c) The resulting velocity model after 3 inversion iterations.**

The updated velocity model provides new constraints on the crustal architecture

for southwest Idaho. Within the new velocity model crustal thickness is at similar depth

as the Prodehl (1979) model, thickest around the western SRP and hotspot track, and

shallowest beneath the Basin and Range province of Nevada. A large zone of slower velocities is also observed beneath Nevada, extending from the surface to ~20 km depth which is consistent with Prodehl's interpretation. The largest change between the starting and final model are the velocities in the upper 10 km which appear to have dropped by as much as 0.5 km/s. This exemplifies the ability for my receiver function analyses to constrain velocities at mid-crustal or greater depth, but poorly resolve the upper crustal velocities, due to limited ray path coverage and seismic frequencies.

The southern margin of the western SRP lies at roughly 100 km distance in Figure 23c. Near this boundary at 10 km depth, I observe a slight velocity increase of ~0.3 km/s when compared to the region to the south. This velocity increase is either evidence of western SRP downwarping or the lack of intrusive volcanic rocks beneath the western SRP. Wood and Clemens (2002) measured the total western SRP downwarping to be 2.3 km with respect to the margins, close to my observations. Another observation made within the western SRP is the 2 km thick high velocity layer at 4-5 km depth. Perhaps this layer is the reason for the gravitation highs associated with volcanic intrusions in the western SRP (Khatiwada and Keller, 2017).

Comparing the Prodehl (1979) interpretations to my receiver function results (Figure 24), we see many similarities in addition to other features. I propose that receiver function analysis can be a cost and time effective method of complimenting large scale active source seismic surveys. The only issues with receiver function analysis are their limited ability to image shallow crustal features (upper 10 km), due to the thin aperture of piercing points, and the ability to image thin (less than 2 km) structures because of the

measured seismic frequencies. With denser station spacing, it would be possible to better

resolve these shallow crustal features and possibly outperform active source surveys.
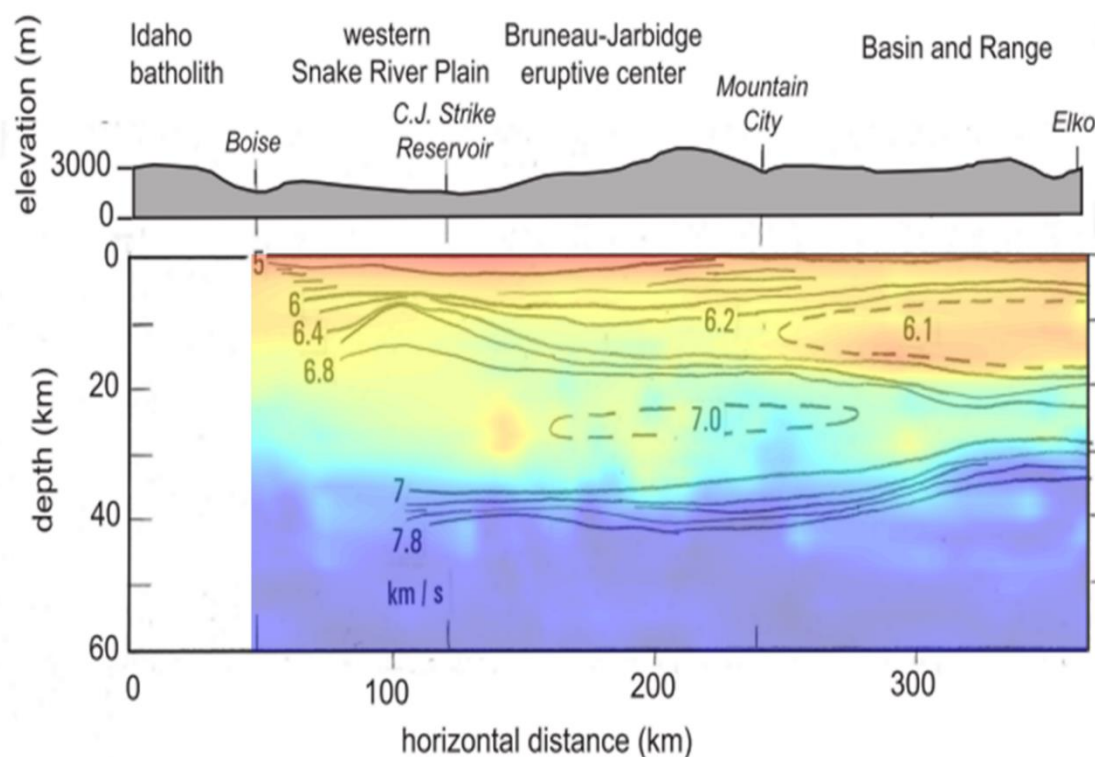
Figure 24.   **The Prodehl (1979) interpretation of the Hill and Pakiser (1967) seismic refraction survey with velocities derived from receiver function inversion overlain upon the figure.**

Geothermal Implications

By utilizing receiver functions to extract crustal velocity distributions, low

velocity zones in the middle or lower crust that represent partial melt materials are

identified with P-wave reflection phase reversals. These velocity reversals are difficult to

constrain or resolve with a traditional (limited seismic source) refraction survey. These

velocity inversions could be related to partially melted sills or dikes that have been

emplaced from the passage of the Yellowstone hotspot. Through my analysis, I have

located areas of anomalously slow seismic velocity that I correlate with the high heat flow that we see in areas of southern Idaho.

In Figure 19, a NEN-SWS trending low velocity zone of 5.5 km/s could be related to partial melt that coincides with the current location of the Yellowstone hotspot. Smith et al., (2009) estimated that this magma reservoir contains 8% -15% partial melt and Huang et al. (2015) estimated this magma reservoir to have a volume of ~10,000 km^3. This demonstrates that large areas of partial melt can been imaged through inverting receiver functions for seismic velocity.

Earlier in this chapter, I interpret possible dikes along the southern margin of the western SRP that extend from 10 to 30 km depth. These dikes are also coincident with a high heat flow region (Figure 5). This may link these mid to lower crustal dikes to the high heat flow of the southern margin of the western SRP. The large abundance of Quaternary faults in this region act as conduits for heat transportation from lower crustal depths to the near surface.

The two active geothermal power plants in my study region are the Raft River and Neal Hot Springs plants. Both of these power plants are coincident with thin crust (25-30 km) and show no signature of partial melt within the crust related to slow velocities. With this information, the heat flow from these power plants is most likely driven by crustal thinning rather than partial melt or radioactive decay within the crust.

Geologic Interpretations

Figures 25, 26, and 27 display the geologic interpretations of cross sections B, D and the Hill and Pakiser line, respectively (Figures 2, 23, and 24). Cross section B extends from the HLP province, through the southern margin of the western SRP and

hotspot track, into the Basin and Range province of Nevada and Utah (Figure 25).

Velocities of 5.3 km/s are observed from the surface to 5 ±2 km depth beneath the

volcanic provinces of Oregon and Idaho. These velocities are related to the mafic

Neogene volcanic rocks of the region and are slower velocities than adjacent areas.

Within the Basin and Range province, I identify a 5.5 km/s layer from the surface to

about 2 km depth that is consistent in thickness and velocity with the Lerch et al. (2007)

interpretation of Paleozoic and Mesozoic sediments. Beneath the SRP, I identify a 5-10

km thick mid-crustal sill. Based on velocity and depth, the composition of this sill is

likely diorite, consistent with the DeNosaquo et al. (2009) gravity derived model. I

interpret the narrow, anomalously slow velocities to be volcanic intrusions, possibly

partially melted dikes of mafic composition. These velocities are faster than the 8-15%

partial melt beneath Yellowstone, but slower than surrounding rocks by 0.5 km/s. The

location of these dikes align with high total magnetic field values along the southern

margin of the WSRP that is also coincident with heat flow values (Figure 3 and 5).
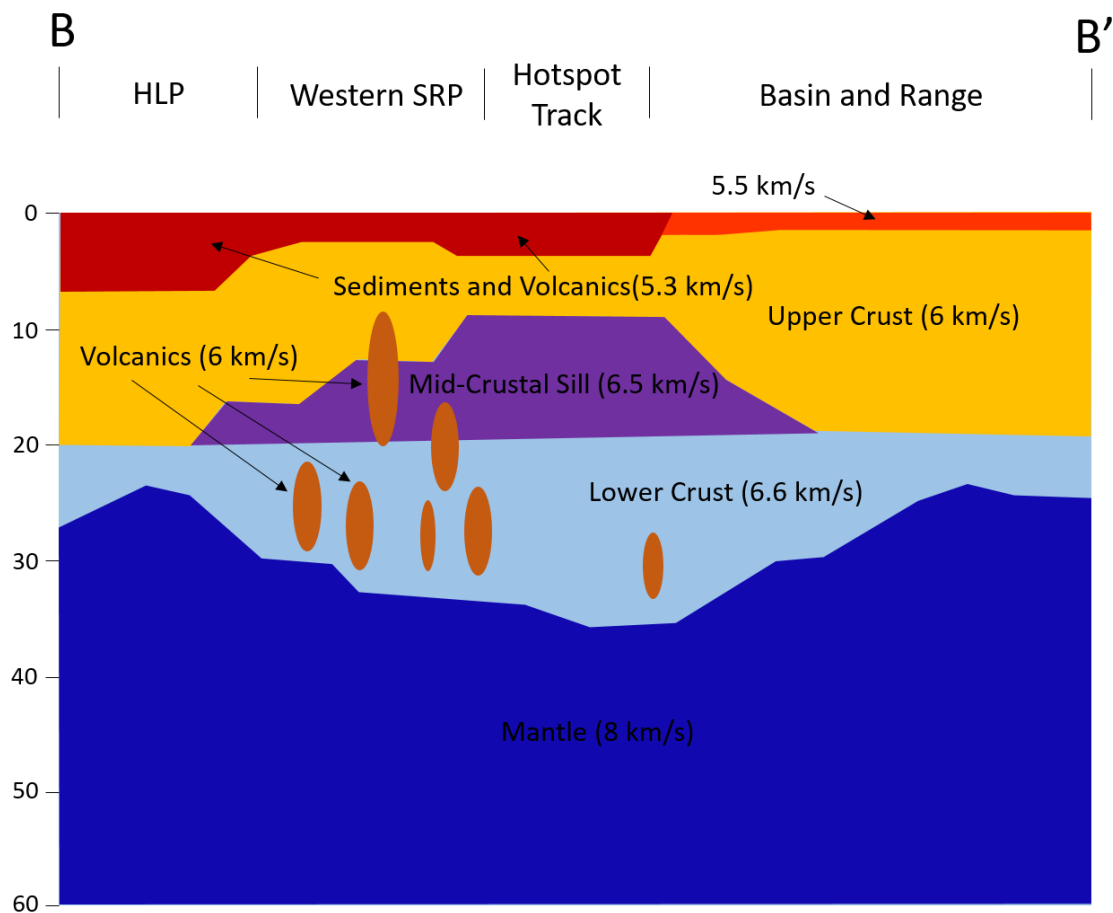
Figure 25. **Schematic of the interpreted geology beneath line B-B' determined from the inversion of receiver function for seismic velocity.**

Along cross section D, I observe many velocity anomalies beneath the topographic expression of the ESRP (hot spot track) compared to the surrounding regions (Figure 26). A velocity of 5.3 km/s in the upper 5 km depth can be related to the Neogene volcanic rocks. A 5-10 km thick high velocity zone has been interpreted as a dioritic mid-crustal sill from 8-15 km depth (Denosaquo et al., 2009). A low velocity zone that can be related to mafic partial melt is seen at the base of the lower crust. These low velocity partial melts are prevalent at the base of the crust beneath most of the eastern SRP as

observed in line H-H' as well as mentioned by Peng and Humphreys (1998) and Denosaquo et al. (2009).
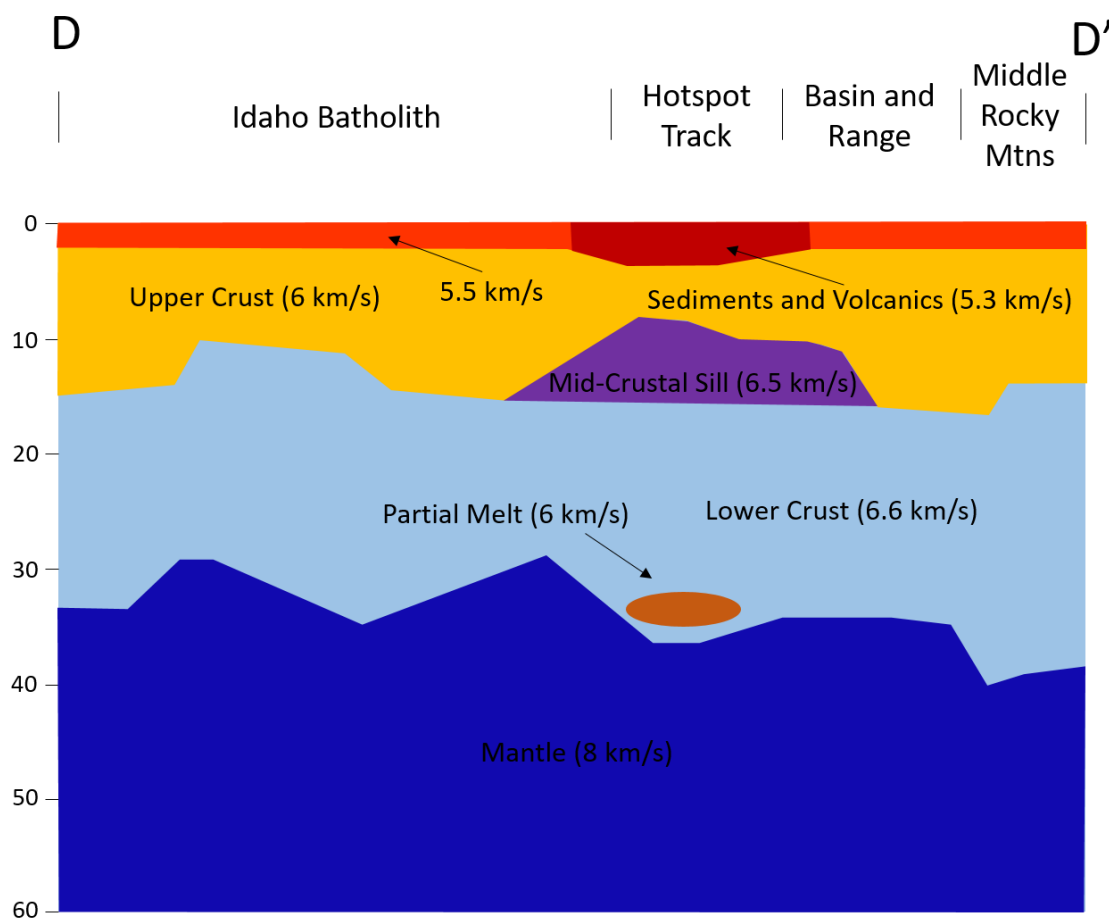
Figure 26.   Schematic of the interpreted geology beneath line D-D' determined from the inversion of receiver function for seismic velocity.

By utilizing both receiver functions and seismic refraction data, I have developed new interpretations for the Hill and Pakiser (1967) seismic refraction line (Figure 27). Within the upper to mid-crust of the western SRP, there is evidence of mid-crustal sills. This is plausible because it is believed that the western SRP exists because of the injection of basaltic magma into the mid-crust (Baldridge et al., 1995; Wood and Clemens, 2002). Areas of low velocity in the lower crust are also observed that can be

related to partial melt. These velocities are greater than the identified mid-crustal magma chamber beneath Yellowstone, but slower than the cooled mid-crustal sills identified beneath the ESRP.
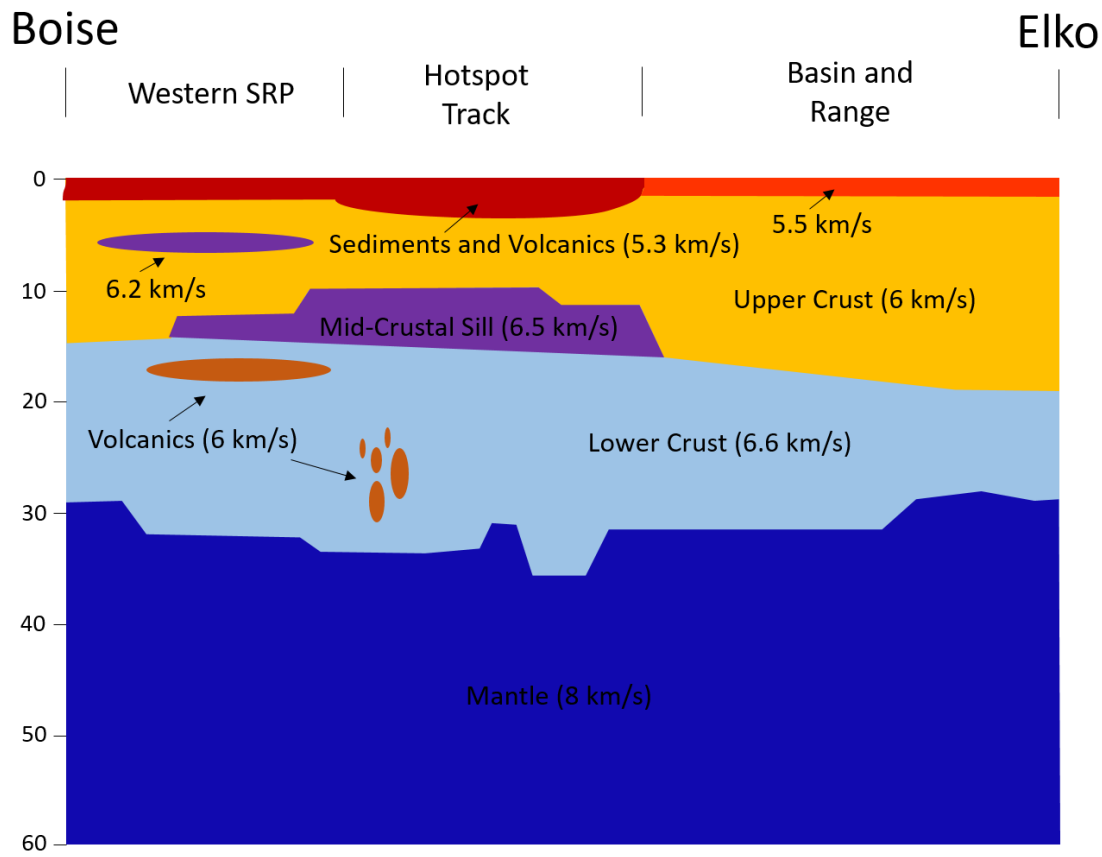
Figure 27. **Schematic of the interpreted geology beneath the Hill and Pakiser (1967) seismic refraction line. These interpretations came from inverting the refraction travel times for seismic velocity using the results from receiver functions as constraints.**

CHAPTER FIVE: CONCLUSIONS

Because of the large velocity contrast between the crust and upper mantle, receiver functions are commonly used to study crustal thickness by locating signals that reflect from the Moho. While this has proved useful to examine lithospheric scale processes, other signals are often ignored within the waveform that represent regional structures within the crust. These crustal structures are typically imaged through large scale refraction surveys that require large explosions and are difficult to permit. To locate finer structure, I invert receiver function waveforms to estimate seismic velocity distributions within the upper 60 km. I employ a Metropolis algorithm approach to the geologically complex region beneath southern Idaho to test the sensitivity of this approach, compare with previous studies, and to identify and characterize the seismic properties.

By inverting receiver functions to derive seismic velocities, I am able to resolve many lithospheric features. Features related to crustal thickness include: (1) a 5-10 km increase in Moho depth along the track of the Yellowstone hotspot; (2) shallow Moho measurements around the Oregon-Idaho graben and the Basin and Range province associated with crustal thinning; (3) a 12 km increase in crustal thickness along the transition zone from the Basin and Range province to the Middle Rocky Mountains.

Due to the volcanic history of southern Idaho, I identify a zone of mid-crustal mafic intrusions along the track of the Yellowstone hotspot. This observation is consistent with the emplacement of dioritic mid-crustal sills that others have identified. I

also identify anomalous seismic velocities beneath the western SRP, but the velocity anomalies are thinner compared to beneath the ESRP. Beneath the current location of the Yellowstone hotspot, I observe slow velocities at depths that coincide with a magma body, consistent with other studies. Within the lower crust beneath the southern margin of the western SRP, I identify vertically oriented, ~15 km wide, low velocity zones that are resolved from multiple earthquake events. These slow features are coincident with a region of high heat flow and high magnetic susceptibility that are tied to dikes that formed from extension of the WSRP. Evidence of a layer of partial melt that lies at the base of the crust beneath most of the eastern SRP is also interpreted.

Applying the results from my receiver function inversions, I provide constraints on deep seated heat sources for most of the southern Idaho geothermal systems. The Weiser area likely has high heat flow due to the crustal thinning that is observed beneath the Oregon-Idaho graben. This supplies the heat necessary to power the Neal Hot Springs geothermal power plant in eastern Oregon. Much of the heat flow in the western SRP/Owyhee region could be generated from partially melted dike or sill complexes in the lower to mid-crust. An abundance of Quaternary faults that lie along the southern margin of the western SRP likely act as a conduit that supplies this heat to the upper few kilometers. I also find supporting evidence that the heat flow of southeastern Idaho and Yellowstone is produced from crustal thinning and a magma reservoir, respectively.

By utilizing a seismic refraction dataset by Hill and Pakiser (1967), I use my receiver function velocity model as a constraint for a new refraction inversion. The new velocity model exhibits some similarities as previous interpretations, but also yield some new features such as mid-crustal sills. This exhibits that lithospheric structure can be

resolved without large-scale, high-cost, and labor intensive seismic refraction surveys. However, due to higher resolution signals and denser station spacing, the active source results best constrain the upper 5 km of the crust. I show that these methods can complement each other by using receiver function based velocity models as a starting model for refraction inversions.

REFERENCES

Albuquerque Seismological Laboratory (ASL)/USGS (1980): US Geological Survey Networks. International Federation of Digital Seismograph Networks. Other/Seismic Network. 10.7914/SN/GS

Albuquerque Seismological Laboratory (ASL)/USGS (1990): United States National Seismic Network. International Federation of Digital Seismograph Networks. Other/Seismic Network. 10.7914/SN/US

Albuquerque Seismological Laboratory (ASL)/USGS (2003): Intermountain West Seismic Network. International Federation of Digital Seismograph Networks. Other/Seismic Network. 10.7914/SN/IW

Ammon, C. J. (1991). The Isolation of Receiver Effects from Teleseismic P Waveforms. Bulletin of the Seismological Society of America, 81(6), 2504–2510. https://doi.org/10.1029/2005JB004161

Anders, M. H., Geissman, J. W., Piety, L. A., and Sullivan, T. J. (1989). Parabolic distribution of circumeastern Snake River Plain seismicity and latest Quaternary faulting: migratory pattern and association with the Yellowstone hotspot. Journal of Geophysical Research, 94(B2), 1589–1621. https://doi.org/10.1029/JB094iB02p01589

Anders, M. H., Rodgers, D. W., Hemming, S. R., Saltzman, J., DiVenere, V. J., Hagstrum, J. T., Embree, G.F., and Walter, R. C. (2014). A fixed sublithospheric source for the late Neogene track of the Yellowstone hotspot: Implications of the Heise and Picabo volcanic fields. *Journal of Geophysical Research: Solid Earth*, 119(4), 2871-2906.

Armstrong, R., Leeman, W., and Malde, H. (1975). K-Ar dating, Quaternary and Neogene volcanic rocks of the Snake River Plain, Idaho. *American Journal of Science*, 275, 225–251.

Baldridge, W.S., Keller G.R., and Braile L.W. (1995). Continental rifting: A final perspective, in K.H. Olsen, ed., Continental Rifts: Evolution, Structure, Tectonics: Elsevier Science, 453-459.

Birch, F. (1964). Density and Composition of Mantle and Core. *Journal of Geophysical Research*, 69.

Blackwell, D.D. (1989). Regional implications of heat flow of the Snake River Plain, Northwestern United States. *Tectonophysics,* 164, 323-343.

Bonnichsen, B., Christiansen, R., Morgan, L., Moye, F., Hackett, W., Leeman, W., Honjo, N., Jenks M., and Godchaux, M. (1989). Excursion 4A: Silicic volcanic rocks in the Snake River Plain-Yellowstone Plateau Province, *in* C.E. Chapin and J. Zidek, eds., Field Excursions to Volcanic Terranes of the Western United States, v. II, Cascades and Intermountain West: New Mexico Bureau of Mines and Mineral Resources Memoir 47, 135-182.

Bonnichsen, B., White, C., Godchaux, M. (1997). Basaltic volcanism, western Snake River Plain [section within Mike McCurry, Bill Bonnichsen, Craig White, M.M. Godchaux, and S.S. Hughes, 1997, Bimodal basalt-rhyolite magmatism in the central and western Snake River Plain, Idaho and Oregon, in P.K. Link and B.J. Kowallis, Proterozoic to Recent Stratigraphy, Tectonics, and Volcanology, Utah, Nevada, Southern Idaho and Central Mexico: Brigham Young University Geology Studies, 42, pt. 1, 381-422], 399-422

Bonnichsen, B., Leeman, W., Honjo, N., McIntosh, W., and Godchaux, M. (2008). Miocene silicic volcanism in southwestern Idaho: geochronology, geochemistry, and evolution in the central Snake River Plain. *Bulletin of Volcanology*, 70(3), 315–342. doi:10.1007/s00445-007-0141-6.

Bradford, J., Mclennan, J., Moore, J., Glasby, D., Waters, D., Kruwell, R., Bailey, A., Rickard, W., Bloomfield, K., and King, D. (2013). Recent Developments at the

Raft River Geothermal Field. Thirty-Eighth Workshop on Geothermal Reservoir Engineering.

Braile, L., Smith, R., Keller, G., Welch, R., and Meyer, R. (1974). Crustal structure across the Wasatch Front from detailed seismic refraction studies. Journal of Geophysical Research, 79(17), 2669–2677. https://doi.org/10.1029/JB079i017p02669

Braile, L., Smith, R., Ansorge, J., Baker, M., Sparlin, M., Prodehl, C., Schilly, M., Healy, J., Mueller, S., and Olsen, K. (1982). The Yellowstone-Snake River Plain seismic pro-filing experiment: Crustal structure of the Eastern Snake River Plain: *Journal of Geophysical Research: Solid Earth*, 87, 2597–2609.

Brook, C., Mariner, R., Mabey, D., Swanson, J., Guffanti, Marianne, and Muffler, L. (1979). Hydrothermal convection systems with reservoir temperatures ~90°C, in Muffler, L. J. P., ed., Assessment of geothermal resources of the United States-1978: U.S. Geological Survey Circular 790, 18--85.

Brueseke, M., Heizler, M., Hart, W., and Mertzman, S. (2007). Distribution and geochronology of Oregon Plateau (U.S.A.) flood basalt volcanism: the Steens Basalt revisited. *Journal of Volcanology and Geothermal Research*, 161, 187–214, doi:10.1016/j.jvolgeores.2006.12.004.

Camp, V., and Ross, M. (2004). Mantle dynamics and genesis of mafic magmatism in the intermontane Pacific Northwest. *Journal of Geophysical Research*, 109, B08204, doi:10.1029/ 2003JB002838.

Carlson, R. and Hart, W. (1987). Crustal genesis on the Oregon Plateau. *Journal of Geophysical Research*, 92, 6191–6206.

Christensen, N. I. and Mooney, W. D. (1995). Seismic velocity structure and composition of the continental crust: A global view. Journal of Geophysical Research, 100(B7), 9761–9788.

Christiansen, R. L. (2001). The Quaternary and Pliocene Yellowstone Plateau volcanic field of Wyoming, Idaho, and Montana. U. S. Geological Survey Professional Paper (Vol. 729–G). https://doi.org/10.3133/PP729G

Clemens, D. and Wood, S. (1991). K-Ar age of silicic volcanic rocks within the lower Columbia River Basalt Group at Timber Butte, Boise and Gem counties. *Isochron/West*, 57(July), 3–7.

Clemens, D. (1993) Tectonics and silicic volcanic stratigraphy of the western Snake River Plain, Idaho. Arizona State University, M.S. thesis, 209 p.

Clemens, D. M., and Wood, S. H. (1993). Radiometric dating, volcanic stratigraphy, and sedimentation in the Boise foothills, northeastern margin of the western Snake River Plain, Ada county, Idaho. *Isochron/West*, 59, 3–10.

Cox, C., Keller, G., and Harder, S. (2013). A controlled-source seismic and gravity study of the High Lava Plains (HLP) of Eastern Oregon. *Geochem. Geophys. Geosyst.*, 14(12), 5208–5226. https://doi.org/10.1002/2013GC004870

Crotwell, H. P. and Owens, T. J. (2005). Automated Receiver Function Processing. *Seismological Research Letters*, 76(6), 702–709. https://doi.org/10.1785/gssrl.76.6.702

Cummings, M., Evans, J., Ferns, M., and Lees K. (2000). Stratigraphic and structural evolution of the middle Miocene synvolcanic Oregon-Idaho graben. *Geological Society of America Bulletin*, 112, 668-682.

Davenport, K. K. (2016). Continental Tectonics from Dense Array Seismic Imaging: Intraplate Seismicity in Virginia and a Steep Cratonic Margin in Idaho. Virginia Polytechnic Institute and State University.

Davenport, K., Hole, J., Tikoff, B., Russo, R., and Harder, S. (2017). A strong contrast in crustal architecture from accreted terranes to craton, constrained by controlled-source seismic data in Idaho and eastern Oregon. *Lithospher*e, 9(2), 325–340. https://doi.org/10.1130/L553.1

DeNosaquo, K. R., Smith, R. B., and Lowry, A. R. (2009). Density and lithospheric strength models of the Yellowstone-Snake River Plain volcanic system from gravity and heat flow data. *Journal of Volcanology and Geothermal Research*, 188(2009), 108–127. https://doi.org/10.1016/j.jvolgeores.2009.08.006

Dueker, K., Humphreys, G. (1997). An asthenosphere-lithosphere probe in North America. International Federation of Digital Seismograph Networks. Other/Seismic Network. 10.7914/SN/XL_1997

Dueker, K., and Sheehan, A. (1997). Mantle discontinuity structure from midpoint stacks of converted P to S waves across the Yellowstone hotspot track. *Journal of Geophysical Research: Solid Earth*, 102(B4), 8313–8327. https://doi.org/10.1029/96JB03857

Dueker, K., Humphreys, G., Smith, R. (2000): Geodynamics of the Yellowstone Hotspot from Seismic and GPS imaging. International Federation of Digital Seismograph Networks. Other/Seismic Network. 10.7914/SN/XC_2000

Eagar, K. C. (2010). Teleseismic Receiver Function Imaging of the Pacific Northwest, United States. Arizona State University.

Eagar, K., Fouch, M., James, D., and Carlson, R. (2011). Crustal structure beneath the High Lava Plains of eastern Oregon and surrounding regions from receiver function analysis. *Journal of Geophysical Research: Solid Earth*, 116(2), 1–18. https://doi.org/10.1029/2010JB007795

Ekren, E.B., McIntyre, D.H., Bennett, E.H., and Malde, H.E. (1981). Geologic map of Owyhee County, Idaho, west of longitude 116°W: U.S. Geological Survey Miscellaneous Investigations Series Map I-1256, scale 1:125 000.

Fitzgerald, J. F. (1982). Geology and Basalt Stratigraphy Weiser Embayment , West-Central. Cenozoic Geology of Idaho, Idaho Bureau of Mines and Geology Bulletin, 26, 103–128.

Fleischmann, D. (2006). Geothermal development needs in Idaho, Geothermal Energy Association.

Geist, D. and Richards (1993). M. Origin of the Columbia Plateau and Snake River plain: deflection of the Yellowstone plume. *Geology*, 21, 789–792.

Giorgis, S., Tikoff, B., McClelland, W. (2005). Missing Idaho arc: transpressional modification of the ^{87}Sr/^{86}Sr transition on the western edge of the Idaho batholith. *Geology,* 33, 469–472.

Giorgis, S., McClelland, W., Fayon, A., Singer, B., and Tikoff, B. (2008). Timing of deformation and exhumation in the western Idaho shear zone, McCall, Idaho. *Bull. Geol. Soc. Am.*, 120, 1119–1133, doi:10.1130/B26291.1.

Glen, J. and Ponce, D. (2002). Large-scale fractures related to inception of the Yellowstone hotspot. *Geology*, 30(7), 647–650. https://doi.org/10.1130/00917613(2002)030<0647:LSFRTI>2.0.CO;2

Gripp, A., and Gordon, R. (2002). Young tracks of hotspots and current plate velocities. *Geophysical Journal International*, 150(2), 321–361. https://doi.org/10.1046/j.1365-246X.2002.01627.x

Hart, W, and Carlson, R. (1987). Tectonic controls on magma genesis and evolution in the northwestern United States. *Journal of Volcanology and Geothermal Research*, 32, 119–135.

Hill, D. P. (1963). Gravity and crustal structure in the western Snake River Plain, Idaho. J. Geophysical Research, 68, 5807-5819.

Hill, D., and Pakiser, L. (1967). Seismic-Refraction Study of Crustal Structure between the Nevada Test Site and Boise, Idaho. U.S. Geological Survey, 78(June), 685–704.

Hooper, P. and Swanson, D. (1990). The Columbia River Basalt Group and associated volcanic rocks of the Blue Mountains Province: U.S. Geological Survey Professional Paper 1437, 63-99.

Hooper, P., and Hawkesworth, C. (1993). Isotopic and geochemical constraints on the origin and evolution of the Columbia River basalt. *Journal of Petrology*, 34, 1203-1246.

Huang, H., Lin, F., Schmandt, B., Farrell, J., Smith, R. B., and Tsai, V. C. (2015). The Yellowstone magmatic system from the mantle plume to the upper crust. Science, 348(6236), 773–776.

Hyndman, D., (1983). The Idaho batholith and associated plutons, Idaho and Western Montana, in Roddick, J. A., editor, Circum-Pacific Pluntonic Terranes: Geologic Society of America Memoir, 159, 213-240.

IRIS DMC (2011), Data Services Products: EMC, A repository of Earth models, https://doi.org/10.17611/DP/EMC.1.

IRIS DMC (2014). Data Services Products: DNA13, P- and S-velocity models for the western US integrating body- and surface-wave constraints, https://doi.org/10.17611/DP/9991615.

Jacobsen, B. H. and Svenningsen, L. (2008). Enhanced uniqueness and linearity of receiver function inversion. *Bulletin of the Seismological Society of America*, 98(4), 1756–1767. https://doi.org/10.1785/0120070180

James, D. and Fouch, M. (2006). Collaborative Research: Understanding the causes of continental intraplate tectonomagmatism: A case study in the Pacific Northwest. International Federation of Digital Seismograph Networks. Other/Seismic Network. 10.7914/SN/XC_2006

Jansson, T. (2008). Receiver function modeling: Modeling local subsurface velocity structures using multiple diverse algorithms. University of Copenhagen.

Jordan, B., Grunder, A., Duncan, R., and Deino, A. (2004) Geochronology of age-progressive volcanism of the Oregon High Lava Plains: Implications for the plume interpretation of Yellowstone. *Journal of Geophysical Research*, 109, B10202, doi:10.1029/2003JB002776.

Kennett B.L.N., Engdahl E.R. and Buland R. (1995). Constraints on seismic velocities in the earth from travel times. *Geophysics Journal International*, 122, 108-124.

Khatiwada, M., and Keller, G. R. (2017). A crustal-scale integrated geophysical and tectonic study of the Snake River Plain region, northwestern U.S.A. *International Geology Review*, DOI: 10.1080/00206814.2017.1303647

Klemperer, S., Miller, K. (2010). Collaborative Research: 4D multi-disciplinary investigation of highly variable crustal response to continental extension in the north-central Basin and Range. International Federation of Digital Seismograph Networks. Other/Seismic Network. 10.7914/SN/YX_2010

Langston, C. A. (1979). Structure under Mount Rainier, Washington, inferred from teleseismic body waves, *J. Geophys. Res.*, 84, 4749-4762.

Lerch, D. W., Klemperer, S. L., Glen, J. M. G., Ponce, D. A., Miller, E. L., and Colgan, J. P. (2007). Crustal structure of the northwestern Basin and Range Province and its transition to unextended volcanic plateaus. Geochemistry, Geophysics, Geosystems, 8(2). https://doi.org/10.1029/2006GC001429

Levin, V., Long, M., Skryzalin, P., Li, Y., and López, I. (2018). Seismic evidence for a recently formed mantle upwelling beneath New England. *Geology*, 46(1), 87–90. https://doi.org/10.1130/G39641.1

Lewis, R., and Stone, M. (1988). Geohydrologic data from a 4,403-foot geothermal test hole, Mountain Home Air Force Base, Elmore County, Idaho: U.S. Geological Survey Open-file Report 88-166, 30.

Ligorría, J. P. and Ammon, C. J. (1999). Iterative deconvolution and receiver function estimation. Bulletin of the Seismological Society of America, 89(October), 1395–1400.

Litherland, M. M. and Klemperer, S. L. (2017). Crustal structure of the Ruby Mountains metamorphic core complex, Nevada, from passive seismic imaging. *Geosphere*, 13(5), 1506–1523. https://doi.org/10.1130/GES01472.1

Mabey, D. (1983). Geothermal Resources of Southern Idaho. Geological Survey Circular 866.

Manduca, C., Silver, L., and Taylor, H. (1992). 87Sr/86Sr and 18O/16O isotopic systematics and geochemistry of granitoid plutons across a steeply-dipping boundary between contrasting lithospheric blocks in western Idaho. *Contrib. Mineral. Petrol.*, 109, 355–372, doi:10.1007/ BF00283324.

Manduca, C., Kuntz, M., and Silver, L. (1993). Emplacement and deformation history of the western margin of the Idaho batholith near McCall, Idaho: Influence of a major terrane boundary, *Geol. Soc. Am. Bull.*, 105, 749–765, doi:10.1130/0016-7606(1993)105<0749: EADHOT>2.3.CO;2.

McIntyre, D. (1979) Preliminary description of Anschutz Federal No. 1 drill hole, Owyhee County, Idaho: U.S. Geological Survey Open- File Report 79-651, 15.

McQuarrie, N., and D. Rodgers (1998), Subsidence of a volcanic basin by flexure and lower crustal flow: The eastern Snake River Plain, Idaho, *Tectonics*, 17, 203–220, doi:10.1029/97TC03762.

Menke, W., Skryzalin, P., Levin, V., Harper, T., Darbyshire, F., and Dong, T. (2016). The Northern Appalachian Anomaly: A modern asthenospheric upwelling. *Geophysical Research Letters*, 43(19), 10,173-10,179. https://doi.org/10.1002/2016GL070918

Metropolis, N., Rosenbluth, A. W., Rosenbluth, M. N., Teller, A. H. and Teller, E. (1953). Equation of state calculations by fast computing machines. *The Journal of Chemical Physics*, 21(6), 1087–1092. https://doi.org/10.1063/1.1699114

Morgan, L., Doherty, D. and Leeman, W. (1984). Ignimbrites of the eastern Snake River Plain: Evidence for major caldera-forming eruptions, *Journal of Geophysical Research*, 89, 8665–8678.

Mosegaard, K. and Tarantola, A. (1995). Monte Carlo sampling of solutions to inverse problems. Journal of Geophysical Research, 100(B7):12431–12447.

Mosegaard, K. and Sambridge, M. (2002). Monte Carlo analysis of inverse problems. Inverse Problems, 18:R29–R54.

Muffler, L., and Guffanti, M. (1979). Assessment of Geothermal Resources of the United States -1978. U.S. Geological Survey (Vol. 790).

Neely, K., and Galinato, G. (2007). Geothermal Power Generation in Idaho: An Overview of Current Developments and Future Potential.

Nelson, P. L., and Grand, S. P. (2018). Lower-mantle plume beneath the Yellowstone hotspot revealed by core waves. Nature Geoscience. https://doi.org/https://doi.org/10.1038/s41561-018-0075-y

Obrebski, M., Allen, R., Xue, M., and Hung, S. (2010). Slab-plume interaction beneath the Pacific Northwest. *Geophysical Research Letters*, 37(14), 1–6. https://doi.org/10.1029/2010GL043489

Owens, T. J., G. Zandt, and S. R. Taylor (1984). Seismic evidence for an ancient rift beneath the Cumberland Plateau, Tennessee: a detailed analysis of broadband teleseismic P waveforms, *J. Geophys. Res*. 89, 7783-7795.

Peng, X. and Humphreys, E. D. (1998). Crustal velocity structure across the eastern Snake River Plain and the Yellowstone swell. *Journal of Geophysical Research*, 103(B4), 7171–7186.

Pierce, L. and K. Morgan (1992). The track of the Yellowstone hot spot: Volcanism, faulting, and uplift, in Regional Geology of Eastern Idaho and Western Wyoming, edited by P. Link, M. Kuntz, and L. Platt, *Mem. Geol. Soc. Am.*, 179, 1–53.

Porritt, R. W., Allen, R. M., and Pollitz, F. F. (2014). Seismic imaging east of the Rocky Mountains with USArray. *Earth and Planetary Science Letters*, 402, 16–25. https://doi.org/10.1016/j.epsl.2013.10.034

Porritt, R. W., and Miller, M. S. (2018). Updates to FuncLab, a Matlab based GUI for handling receiver functions. Computers and Geosciences, 111, 260–271. https://doi.org/10.1016/j.cageo.2017.11.022

Priestley, K. and J. Orcutt. (1982). Extremal travel time inversion of explosion seismology data from the eastern Snake River Plain, Idaho, *Journal of Geophysical Research*, 87, 2634–2642, doi:10.1029/JB087iB04p02634.

Prodehl, C. (1979). Crustal Structure of the Western United States. Geological Survey Professional Paper; 1034.

Schmitz, M., Heinsohn, W. D., and Schilling, F. R. (1997). Seismic, gravity and petrological evidence for partial melt beneath the thickened Central Andean crust (21-23°S). *Tectonophysics*, 270(1997), 313–326. https://doi.org/10.1016/S0040-1951(96)00217-X

Shearer, P.M. (1999). Introduction to Seismology. Cambridge University Press.

Shervais, J., Vetter, S., and Hanan B. (2006). Layered mafic sill complex beneath the eastern Snake River Plain: Evidence from cyclic geochemical variations in basalt, *Geology*, 34, 365–368, doi:10.1130/G22226.1.

Shervais, J., Evans, J., Nielson, D., Glen, J., Liberty, L., Dobson, P., Sonnenthal, E., Gasperikova, E., Siler, D., Visser, C., Garg, S., DeAngelo, J., Athens, N. (2015). Geothermal Play Fairway Analysis, Snake River Plain, Idaho: Phase 1 Report. Geothermal Resource Council Annual Meeting.

Shervais, J., Glen, J., Nielson, D., Garg, S., Dobson, P., Gasperikova, E., Sonnenthal, E., Visser, C., Liberty, L., Evans, J., Liberty, L., DeAngelo, J., Siler, D. and Varriale, J. (2016). Geothermal Play Fairway Analysis of the Snake River Plain, Idaho. 41st Workshop on Geothermal Reservoir Engineering, 1–7.

Smith, R. B., and Sbar, M. L. (1974). Contemporary tectonics and seismicity of the Western United States with emphasis on the Intermountain Seismic Belt. *Bulletin of the Geological Society of America*, 85, 1205–1218. https://doi.org/10.1130/0016-7606(1974)85<1205:CTASOT>2.0.CO;2

Smith, R., Schilly, M., Braile, L., Ansorge, J., Lehman, J., Baker, M., Prodehl, C., Healy, J., Mueller, S., and Greensfelder, R. (1982). The 1978 Yellowstone-eastern Snake River Plain seismic profiling experiment: crustal structure of the Yellowstone region and experiment design: Journal of Geophysical Research: Solid Earth, 87(B4), 2583–2596. 10.1029/JB087iB04p02583

Smith, R. B., Jordan, M., Steinberger, B., Puskas, C. M., Farrell, J., Waite, G. P., Husen, S., Chang, W., O'Connell, R. (2009). Geodynamics of the Yellowstone hotspot and mantle plume: Seismic and GPS imaging, kinematics, and mantle flow. *Journal of Volcanology and Geothermal Research*, 188(2009), 26–56. https://doi.org/10.1016/j.jvolgeores.2009.08.020

Sparlin, M., Braile, L., and Smith, R. (1982). Crustal structure of the eastern snake river plain determined from ray trace modeling of seismic refraction data, *Journal of Geophysical Research: Solid Earth*, 87(B4), 2619– 2633. 10.1029/JB087iB04p02619

Squires, E., Wood, S., and Osiensky J. (1992) Hydrogeologic frame-work of the Boise aquifer system, Ada County, Idaho: Idaho Water Resources Research Institute,

Research Technical Completion Report 14-08-0001-0G1559-06, University of Idaho, 114.

St. Clair, J. (2015). Geophysical investigations of underplating at the Middle American Trench, weathering in the critical zone, and snow water equivalent in seasonal snow, PhD thesis, University of Wyoming.

Stachnik, J., Dueker, K., Schutt, D., and Yuan, H. (2008). Imaging Yellowstone plume-lithosphere interactions from inversion of ballistic and diffusive Rayleigh wave dispersion and crustal thickness data, *Geochemistry, Geophysics, Geosystems*, 9(6). https://doi.org/10.1029/2008GC001992

Stanciu, A., Russo, R., Mocanu, V., Bremner, P., Hongsresawat, S., Torpey, M., VanDecar, J., Foster, D., and Hole, J. (2016). Crustal structure beneath the Blue Mountains terranes and cratonic North America, eastern Oregon, and Idaho, from teleseismic receiver functions. *Journal of Geophysical Research*, 121, 5049–5067. https://doi.org/10.1002/2016JB012989.

Streck, M., and Grunder, A. (2008) Phenocryst-poor rhyolites of bimodal, tholeiitic provinces: The Rattlesnake Tuff and implications for mush extraction models, *Bull of Volcanology*, 70(3), 385–401.

Streck, M. and Grunder, A. (2012). Temporal and crustal effects on differentiation of tholeiite to calcalkaline and ferrotrachytic suites, High Lava Plains, Oregon, USA. *Geochemistry, Geophysics, Geosystems*, 13, Q0AN02, doi:10.1029/2012GC004237.

University of Utah (1962). University of Utah Regional Seismic Network. International Federation of Digital Seismograph Networks. Other/Seismic Network. 10.7914/SN/UU

University of Utah (1984). Yellowstone Wyoming Seismic Network. International Federation of Digital Seismograph Networks. Other/Seismic Network. 10.7914/SN/WY

University of Washington (1963). Pacific Northwest Seismic Network. International Federation of Digital Seismograph Networks. Other/Seismic Network. 10.7914/SN/UW

Walker, K. and Klemperer, S. (2000). Shear-wave Splitting in the Snake River Plain. International Federation of Digital Seismograph Networks. Other/Seismic Network. 10.7914/SN/XJ_2000

Warren, I. (2017). Exploration and Development of the Neal Hot Springs Geothermal Resource, Malheur County, Oregon *. *Search and Discovery Article*, (80584).

Wernicke, B. P., England, P. C., Sonder, L. J., and Christiansen, R. L. (1987). Tectonomagmatic evolution of Cenozoic extension in the North American Cordillera. Geological Society, London, Special Publications, 28(1), 203–221. https://doi.org/10.1144/GSL.SP.1987.028.01.15

Whitehead, R.L. (1992) Geohydrologic framework of the Snake River Plain, Idaho and eastern Oregon: U.S. Geological Survey Professional Paper 1408-B, 32 p.

Wood, S. (1989). Silicic volcanic rocks and structure of the western Mount Bennett Hills and adjacent Snake River Plain, Idaho, in R.P. Smith and K.L. Ruebelmann, eds., Snake River Plain-Yellowstone Volcanic Province: 28th International Geological Congress, Guide- book T305, *American Geophysical Union*, 69- 77.

Wood, S., and Clemens, D. (2002). Geologic and Tectonic History of the Western Snake River Plain, Idaho. *Idaho Geological Survey Bulletin*, 30 (January), 69–103.

Xu, Z. (2018). Personal Communications. Department of Geosciences, Boise State University.

Yang, X., Pavlis, G. L., and Wang, Y. (2016). A quality control method for teleseismic p-wave receiver functions. Bulletin of the Seismological Society of America, 106(5), 1948–1962. https://doi.org/10.1785/0120150347

Yilmaz, Ö. (2001). Seismic data analysis, Society of Exploration Geophysicists, Tulsa, Ok, 2027 p.

Young, H., and Mitchell, J. (1973). Geothermal investigations in Idaho, Part 1, Geochemical and geological setting of selected thermal waters. Idaho Department of Water Administration Water Information Bulletin, 30.

Yuan, H., Dueker, K. (2005). Teleseismic P-wave tomogram of the Yellowstone plume. *Geophys. Res. Lett.*, 32, L07304. doi:10.1029/2004FL022056.

Yuan, H., Dueker, K., and Stachnik, J. (2010). Crustal structure and thickness along the Yellowstone hot spot track: Evidence for lower crustal outflow from beneath the eastern Snake River Plain. *Geochemistry, Geophysics, Geosystems,* 11(3). https://doi.org/10.1029/2009GC002787

Zhu, L. and Kanamori, H. (2000). Moho depth variation in southern California from teleseismic receiver functions. *J. geophys. Res.*, 105, 2969–2980.